HHS Public Access

Author manuscript

Dev Cell. Author manuscript; available in PMC 2023 April 11.

Published in final edited form as:

Dev Cell. 2022 April 11; 57(7): 930–944.e6. doi:10.1016/j.devcel.2022.03.008.

SALSA, a genetically-encoded biosensor for spatiotemporal quantification of Notch signal transduction in vivo

Justin M. Shaffer,

Iva Greenwald*

Dept. of Biological Sciences, Columbia University, New York, NY 10027

Abstract

Notch-mediated lateral specification is a fundamental mechanism to resolve stochastic cell fate choices by amplifying initial differences between equivalent cells. To study how stochastic events impact Notch activity, we developed a biosensor, SALSA (Sensor Able to detect Lateral Signaling Activity), consisting of an amplifying "switch" — Notch tagged with TEV protease — and a "reporter" — GFP fused to a nuclearly-localized red fluorescent protein, separated by a TEV cut site. When ligand activates Notch, TEVp enters the nucleus and releases GFP from its nuclear tether, allowing Notch activation to be quantified based on changes in GFP subcellular localization. We show that SALSA accurately reports Notch activity in different signaling paradigms in *Caenorhabditis elegans*, and use time-lapse imaging to test hypotheses about how stochastic elements ensure a reproducible and robust outcome in a canonical *lin-12/Notch*-mediated lateral signaling paradigm. SALSA should be generalizable to other experimental systems, and adaptable to increase options for bespoke "SynNotch" applications.

eTOC:

Shaffer and Greenwald describe a genetically-encoded biosensor for Notch signal transduction using a visible, quantifiable nuclear to cytoplasmic change in GFP localization. It performed well in different *C. elegans* signaling paradigms and should be applicable to other experimental models and adaptable for modular synthetic Notch receptor (SynNotch) applications.

Graphical Abstract

*Author for correspondence and lead contact, isg4@columbia.edu.

Author Contributions

J.M.S. and I.G. designed the experiments. J.M.S. conducted the experiments and performed all statistical analysis. J.M.S. and I.G. interpreted the data. J.M.S. and I.G. wrote the paper.

Declaration of Interests

The authors declare no competing interests.

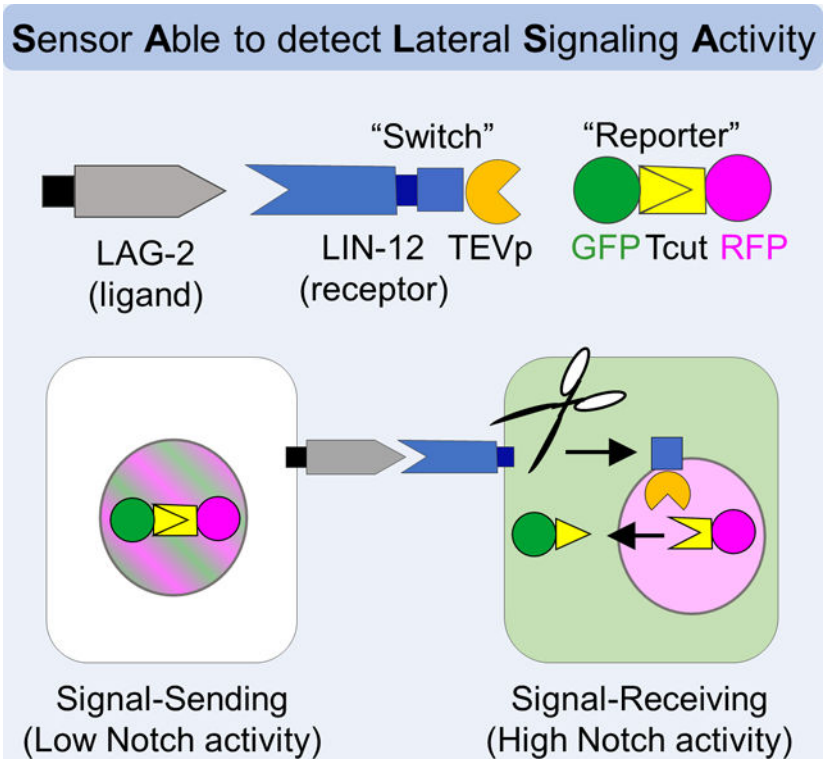

Keywords

C. elegans ; LIN-12; Notch; biosensor; stochastic cell fate; gonad; vulva; germ line; GLP-1

Introduction

Notch signaling plays profound and pervasive roles in development and disease. Notch is one of the major receptors for cell-cell interactions, and uniquely mediates lateral specification (also called lateral inhibition), a process by which initially equivalent cells interact with each other and then adopt different alternative fates. Lateral specification allows for stochastic cell fate decisions to be resolved into reproducible and robust final outcomes. To further our studies of a canonical example of Notch-mediated lateral specification, the Anchor Cell (AC)/Ventral Uterine precursor cell (VU) decision (reviewed in Greenwald, 2012), and test a recent model for the relationship between stochastic events and the outcome of the AC/VU decision (Attner et al., 2019), we needed a way to visualize the onset of LIN-12 signaling and track the relative levels of signaling activity in individual cells over time. However, conventional methods including transcriptional reporters (described herein) are not sensitive enough and lack the temporal resolution required for this purpose,

To accomplish these goals, we developed Sensor Able to detect Lateral Signaling Activity (SALSA), a genetically-encoded biosensor that allows for ratiometric quantitation of nuclear Red:Green fluorescence as a measure of Notch signaling activity. We demonstrate the efficacy and fidelity of SALSA in four different cell fate paradigms using both *C. elegans*

Notch proteins, LIN-12 and GLP-1. By combining SALSA with time-lapse imaging to quantify LIN-12 signaling during the AC/VU decision, we provide evidence in strong support of the recent model for how stochastic events become determinative to ensure a reproducible and robust outcome. Our success in multiple *C. elegans* paradigms suggests that this approach will be generally useful for studies of Notch signaling in other systems. We also discuss potential adaptations based on SALSA to increase the options for customized "SynNotch" applications.

Results

Design

The intracellular domain of Notch is essentially a membrane-tethered transcriptional coactivator. Ligand-binding leads to sequential proteolytic cleavages to release the intracellular domain from its tether; the first, mediated by an ADAM protease, leads to ectodomain shedding and the second, mediated by γ-secretase, occurs within the transmembrane domain. The intracellular domain then translocates to the nucleus and becomes part of a transcriptional activation complex (reviewed in Falo-Sanjuan and Bray, 2020; Greenwald and Kovall, 2013; Henrique and Schweisguth, 2019; Figure 1A). This simple, direct mechanism was the starting point for the development of SALSA (Figure 1B).

***Established assays for quantifying* Notch *activity.*—**Most measurements of Notch activity have relied on transcriptional outputs. For native Notch, these outputs may be natural target gene products or transcriptional reporters incorporating single or multimerized consensus binding sites for the Notch nuclear complex (Hansson et al., 2006; Souilhol et al., 2006; reviewed in Zacharioudaki and Bray, 2014). If the intracellular domain of Notch is instead tagged with, or replaced by, a heterologous transcription factor such as yeast Gal4, nuclear access is revealed by a transcriptional reporter for the heterologous factor (reviewed in Housden et al., 2014; Lecourtois and Schweisguth, 1998; Struhl and Adachi, 1998). However, transcription-based reporters have limitations for the temporal resolution of signaling onset and cessation. Limitations to the on-rate include a lag for visualizing the onset and changes in signal transduction due to the time it takes for sufficient protein encoded by the reporter gene to be transcribed and translated, and in the case of fluorescent proteins used for live imaging, to mature (Bothma et al., 2018); a potential limitation to the off-rate is perdurance of the reporter proteins. In addition, the expression of natural target genes or transgene reporters may be influenced by other inputs from their cellular and/or genomic context.

Available assays based on cleavage and release of the intracellular domain per se do not have these limitations, but have others. In cell culture, luciferase complementation imaging measures Notch nuclear complex formation by fusing the amino terminal fragment of luciferase to the intracellular domain of Notch and the carboxy terminal fragment of luciferase to the CSL protein of the Notch nuclear complex, reconstituting luciferase activity when the complex forms (Ilagan et al., 2011). However, this method is limited by the amount and stability of the nuclear complex, and in *C. elegans*, the ability for the substrate to penetrate the cuticle of intact worms (Sfarcic et al., 2019). These limitations

may be considerable for live imaging in vivo over time because developmentally meaningful signaling is effective at low levels and the Notch intracellular domain is rapidly degraded in the nucleus. Similar limitations also apply to measurements of the nuclear level of the intracellular domain directly tagged with fluorescent proteins. The low native level of cleavage product is particularly problematic for time-lapse imaging in *C. elegans*, as the level of blue-light illumination required for imaging weak signals from GFP-tagged proteins is damaging to animal development (Edwards et al., 2008; Ward et al., 2008).

The low level and instability of the natural cleavage product has been circumvented by replacing the intracellular domain with Cre recombinase and looking for excision of a lox-stop-lox cassette from a target, which permanently marks lineages in which Notch signaling has occurred, and has therefore been valuable for identifying lineages in which Notch has been active (Liu et al., 2015; Vooijs et al., 2007). However, this method is not suitable for quantifying signal transduction in a cell over time, and an earlier event in a lineage would mask a later, independent one.

GPCR and ERK biosensor antecedents.—In designing our ideal Notch biosensor, which would include an amplification step while eschewing a transcriptional readout, we were inspired by features of two other biosensors. One is the “Tango” assay (Barnea et al., 2008; Inagaki et al., 2012; Katow et al., 2019), in which ligand-dependent recruitment of an arrestin::Tobacco Etch Virus protease (TEVp; Kapust et al., 2002) fusion protein releases a transcription factor fused to a second receptor through cleavage of an intervening TEV recognition site (Tcut); the released transcription factor activates expression of a target gene reporter. The other is the ERK-KTR (kinase translocation reporter), which converts ERK activity into a change in nucleocytoplasmic localization of KTR::Clover (Regot et al., 2014); when expressed as a bicistronic transcript with a nuclear-tethered red fluorescent protein, ERK activity may be quantified as a Red:Green ratio of nuclear fluorescence, an advantage when cells are small, closely packed together, and change in size, shape, or form syncytia during development, as in *C. elegans* (de la Cova et al., 2017).

Design of SALSA.—SALSA is a bipartite system, consisting of a “switch” and a “reporter” (Figure 1B). For the switch, we used CRISPR/Cas9 to create endogenously-tagged alleles for both *C. elegans* Notch homologs, LIN-12 and GLP-1, that encode TEVp fused to the carboxy terminus of the intracellular domain (STAR Methods). Homozygotes for the switch alleles for *lin-12(ar640)* [LIN-12::TEVp] and *glp-1(ar648)* [GLP-1::TEVp] are viable, fertile, and phenotypically indistinguishable from wild type, indicating that the tagged proteins are fully functional (STAR Methods). When GFP is added to endogenous LIN-12 at the same position, the animals also appear phenotypically wild-type, and LIN-12::GFP is observed primarily at the cell surface as expected, indicating that trafficking is not compromised (Attner et al., 2019; Chan, 2020); GFP and other tags placed at or near the carboxy terminus of GLP-1 also appear functional and permit proper trafficking (Sorensen et al., 2020). The use of endogenous *lin-12* and *glp-1* allowed us to measure the level of signaling during cell fate decisions with potential regulatory mechanisms intact, including rapid turnover of the untethered intracellular domain::TEVp fusion by regulators such as the E3 ubiquitin ligase SEL-10/Fbxw7 (de la Cova and Greenwald, 2012; Deng and

Greenwald, 2016; Hubbard et al., 1997), which should also lead to degradation of the TEVp moiety. Alternate transgenic switch designs and applications are described in the Discussion.

The reporter is a substrate for TEVp: GFP coupled to an RFP::H2B (here, usually mScarlet), separated by a linker containing the recognition site for TEVp (GFP::Tcut::RFP::H2B) (STAR Methods). The cleavage state of the reporter will reflect the subcellular localization of TEVp: when Notch is inactive, TEVp is tethered to the membrane and GFP remains attached to RFP::H2B in the nucleus; when Notch is activated, TEVp enters the nucleus and cleaves the reporter, allowing GFP to diffuse out of the nucleus. Thus, Notch signaling activity can be quantified as a "Red:Green" ratio of RFP ("Red"):GFP ("Green") fluorescence in the nucleus, (using RFP as the nuclear segmentation marker, Figure 1B; for other ratios that can be used, see Figure S3). This cleavable reporter was able to distinguish cells with active Notch signal transduction from cells with inactive Notch signal transduction in live worms, and allowed for the cumulative increase in signal transduction to be observed over time during the AC/VU decision.

We note that we did not observe fluorescence resonance energy transfer (FRET) or photoconversion of mScarlet using this reporter design, and that addition of nuclear export signal (NES) sequences to the GFP proved to be problematic to the cells of interest (see STAR Methods). We also note that we expressed the cleavable reporter tissue-specifically to simplify image collection and cell identification (de la Cova et al., 2017), although tissue-specific expression is not required to implement SALSA.

Testing SALSA in signaling paradigms with stereotyped patterns of Notch activity: Vulval Precursor Cells, the M lineage, and the germ line

We tested the fidelity of SALSA as a readout for Notch signaling activity in different signaling paradigms for which extensive prior genetic studies coupled with target gene transcriptional outputs give confidence about the expected patterns of Notch activity and inactivity at the level of individual cells. In all cases, SALSA faithfully reported activity based on the expectations. Each paradigm offered the opportunity to gain additional insights into the performance of SALSA.

VPCs: measurements with signaling manipulation.—Three VPCs, named P5.p, P6.p, and P7.p, give rise to the vulva (Sulston and Horvitz, 1977). They are initially multipotent, and are patterned in the L3 stage: in wild-type hermaphrodites, the central VPC, P6.p, always adopts the "1°" vulval fate, and the flanking VPCs, P5.p and P7.p, always adopt the "2°" fate (Gauthier and Rocheleau, 2017; Shin and Reiner, 2018; Sternberg, 2005). This fate pattern results when an EGF-like signal from the AC activates EGFR and a canonical Ras cascade in P6.p, inducing it to adopt the 1° fate, downregulate LIN-12 protein levels, and produce the "lateral signal" composed of ligands for LIN-12/Notch (Figure 2A). These ligands activate LIN-12/Notch in P5.p and P7.p, causing them to adopt the 2° vulval fate. In the L3 stage, several LIN-12 target transcriptional reporters are expressed specifically in, or upregulated in, P5.p and P7.p and their descendants, with expression depending on cis-acting binding sites for the LIN-12 nuclear complex (Berset et al., 2001; Luo et al., 2020; Yoo et al., 2004; Yoo and Greenwald, 2005).

We drove expression of the GFP::Tcut::mScarlet::H2B cleavable reporter in VPCs and their descendants (STAR Methods). If SALSA faithfully reports LIN-12 signaling activity, we would expect a high nuclear Red:Green fluorescence ratio in P5.p and P7.p compared to P6.p in the presence of the LIN-12::TEVp switch, and a uniformly low nuclear Red:Green ratio in P5.p, P6.p and P7.p in the absence of the LIN-12::TEVp switch (reporter-only control). These expectations were met (Figure 2B). As a further test of SALSA fidelity, we removed the lateral signal. To do so, we genetically blocked the AC from forming [using *hlh-2(ar614)*; see STAR Methods], thereby removing the source of the EGF-like signal that causes P6.p to express the ligands that normally activate LIN-12 in P5.p and P7.p. If SALSA faithfully reports LIN-12 signaling activity, we would expect that, in the absence of an AC, these three VPCs would have uniformly low nuclear Red:Green ratios even in the presence of the LIN-12::TEVp switch, similar to when the switch is absent. Indeed, we found this to be the case (Figure 2B). Finally, we found that removing the SEL-10 E3 ubiquitin ligase that targets the intracellular domain of LIN-12 for degradation in VPCs increases the nuclear Red:Green ratio, in accordance with expectations (Figure S1).

M lineage: different ratiometric measurements of signal transduction.—The postembryonic mesoblast M generates dorsally-located and ventrally-located descendants that adopt distinct fates based on signals they receive. LIN-12/Notch is necessary to specify ventral cell fates; the relevant signaling begins at the 4-M stage (granddaughters of M), when ligand begins to be expressed by cells adjacent to only the ventral M lineage cells (Foehr and Liu, 2008) (Figure 3A). LIN-12::GFP is expressed at similar levels in the dorsal and ventral cells of the M lineage at the 4-M to 8-M stages (Foehr and Liu, 2008). We evaluated the performance of SALSA in individual worms carrying the LIN-12::TEVp switch and a transgene that expresses the GFP::Tcut::mScarlet::H2B cleavable reporter in M and all of its descendants (STAR Methods). If SALSA faithfully reports LIN-12 signaling activity, we would expect a higher nuclear Red:Green fluorescence ratio in ventral descendants, where M lineage cells are juxtaposed to ligand, than in dorsal descendants, where cells are not exposed to ligand. These expectations were met, as shown in quantification of nuclear Red:Green at the 8-M stage (Figure 3B–D) and in time-lapse movies that show the onset of signaling in ventral cells in the 4-M stage (Figure S2).

The relatively wide spacing between cells at the 8-M stage also allowed us to compare alternate methods for quantifying signal transduction. Of particular note, we were able to use a “cytoring” (Regot et al., 2014) to determine that similar results are obtained using the Cytoplasmic:Nuclear (C:N) fluorescence ratio, which may be advantageous in certain contexts, particularly in other systems where cells are larger or spaced further apart than is generally true in *C. elegans* (see Discussion and Figure S3 legend).

Germ line: GLP-1/Notch SALSA.—The *C. elegans* gonad has two arms that extend outwards from the centrally-located uterus. Ligands produced by the somatic distal tip cell (DTC) at the end of each gonad arm activate GLP-1/Notch in nearby Germline Stem Cells (GSCs) to inhibit entry into meiosis (reviewed in Hubbard and Schedl, 2019). As the proliferating GSCs are displaced proximally out of the GSC niche, they undergo a transition to meiosis. Genetic analysis established that *glp-1* activity is necessary and sufficient to

sustain the GSC fate (Austin and Kimble, 1987; Berry et al., 1997; Priess et al., 1987). In L4 hermaphrodites (Figure 4A), activation of GLP-1 peaks in a zone that extends approximately 5 cell diameters from the DTCs, where there is maximal contact with DTC processes, based on the visualization of the nuclearly-localized intracellular domain of GLP-1 (Gutnik et al., 2018) and *in situ* hybridization or antibody staining for targets of GLP-1 in the germ line (Chen et al., 2020; Kershner et al., 2014; Lee et al., 2016). Transcripts for a direct target of GLP-1 are detected up to ~8–10 cell diameters from the distal end (Chen et al., 2020; Kershner et al., 2014; Lee et al., 2019; Lee et al., 2016), and GLP-1 is expressed throughout (and beyond) the progenitor zone (Crittenden et al., 1994), which ends ~21 cell diameters from the distal end.

We expressed the GFP::Tcut::mCherry::H2B cleavable reporter in all germline cells (STAR Methods), and visualized and quantified fluorescence in L4 hermaphrodites. If SALSA accurately reports GLP-1 activity, we would expect to see visibly reddened germline nuclei at least 5 cell diameters from the distal end of the gonad arm and a low nuclear Red:Green ratio from uncleaved reporter more proximally in the presence of the GLP-1::TEVp switch, and a uniformly low nuclear Red:Green ratio in the absence of the GLP-1::TEVp switch. The appearance of the germ line (Figure 4B) and our quantitative analysis (Figure 4C) conformed to this expectation. In particular, when we quantified the nuclear Red:Green ratio at 0, 5, 10, and 15 cell diameters from the distal end, we found that in the presence of the GLP-1::TEVp switch, the nuclear Red:Green ratio was high at 0 and 5 diameters and low at 10 and 15 cell diameters (Figure 4C), approaching the level of the no-switch control. These results are consistent with expectations based on the evidence for maximal activity extending five cell diameters and the absence of activity beyond the GSC zone.

Because the distance from the DTC in cell diameters represents a temporal progression in which GLP-1 signaling activity decreases as cells are displaced from contact with the DTC, the germ line data also suggest that the “off-rate” of SALSA is relatively responsive to the cessation of GLP-1 activation: there is a low nuclear Red:Green ratio past the GSC region, where GLP-1 target genes appear not to be actively transcribed (Lee et al., 2016; Lee et al., 2019).

Testing SALSA in the AC/VU decision

The LIN-12/Notch-mediated AC/VU decision is a canonical example of lateral specification (reviewed in Greenwald, 2012). The α cells descend from the two somatic gonad precursor cells present at hatching, Z1 and Z4 (Figure 5A). Each α cell is born with the potential to be the sole Anchor Cell (AC), a terminally differentiated cell that organizes development of the uterus and vulva, or a Ventral Uterine precursor cell (αVU), which generates uterine structural cells. In any individual, one α cell becomes the AC and the other becomes the αVU. However, the outcome is stochastic: 50% of the time the α cell descended from Z1 becomes the AC, and the other 50% of the time the α cell descended from Z4 becomes the AC. This decision is precise and robust because the two α cells interact with each other via LIN-12 and its ligand LAG-2 to resolve which will be the AC and which will be the αVU.

lin-12 acts as a classic “switch gene” in mediating the AC/VU decision (Greenwald et al., 1983). Both α cells initially express LIN-12 and LAG-2; genetic and expression studies

suggested that a stochastic initial difference in *lin-12* activity between the two uncommitted α cells becomes amplified by feedback mechanisms, ensuring that the α cell with higher *lin-12* activity continues to express *lin-12*, ceases to express *lag-2*, and becomes the αVU while the other α cell ceases to express *lin-12*, continues to express *lag-2*, and becomes the AC (reviewed in Greenwald, 2012; Figure 5B). When the cells have committed to their fates, the AC expresses only LAG-2 and the αVU expresses only LIN-12. Several readouts of LIN-12 activity are seen in the committed αVU and not in the AC in the early L3 stage: (i) nuclear GFP produced after cleavage of endogenous LIN-12::GFP (Attner et al., 2019), (ii) the transcriptional reporter *arIs107[mir-61p::2xnls::yfp]* (Yoo and Greenwald, 2005), and (iii) positive autoregulation of endogenous *lag-1::gfp*, the CSL protein in *C. elegans* (Luo et al., 2020). Transcriptional reporters containing multimerized CSL binding sites are not expressed in the somatic gonad (or VPCs) (e.g. Li, 2011) so cannot be used to follow LIN-12 activation.

We tested whether the readout of SALSA conforms to expectations by examining the specified AC and αVU in the L3 stage (Figure 5B). To implement SALSA in the somatic gonad, we used a variation on "*lox-stop-lox*" called Flexon (Shaffer and Greenwald, 2022) to express GFP::Tcut::mScarlet::H2B strongly, specifically, and constitutively in all somatic gonadal cells (Figure 5C) under the control of a ribosomal protein gene promoter (*rps-27p*), thereby avoiding transcriptional regulatory mechanisms that operate in the AC/VU decision (Wilkinson et al., 1994). One transgene, *arTi237,* drives expression of Cre recombinase specifically in the somatic gonad precursor cells Z1 and Z4; the other, *arTi355*, contains a *flexon* stop cassette that prevents expression of the GFP::Tcut::mScarlet::H2B cleavable reporter from *rps-27p* unless Cre-mediated excision of the *flexon* occurs (Figure 5C; STAR Methods). Excision is very efficient in Z1 and Z4, the great-grandparents of the α cells, (Shaffer and Greenwald, 2022), so the cleavable reporter is strongly and uniformly expressed in both α cells in all animals. Hereafter, we refer to the combination of these two transgenes as the "somatic gonad cleavable reporter."

When we quantified the somatic gonad cleavable reporter in the AC and αVU, we observed a significantly higher nuclear Red:Green ratio in the αVU than in the AC in the presence of the LIN-12::TEVp switch (Figure 5D), and a similar, low nuclear Red:Green ratio in both the AC and αVU in the cleavable reporter-only control (Figure 5E), indicating that SALSA is an accurate reporter of *lin-12* activity in this context.

SALSA illuminates the relationship between birth-time interval and relative birth order at the outset of the AC/VU decision

High-throughput lineage analysis identified two inter-related stochastic events that *precede* the AC/VU decision and predict its outcome (Attner et al., 2019). The first stochastic element is the relative birth order of the α cells: one of the α cells is usually born before the other, so there is a "first-born" α cell and a "second-born" α cell. When the birth-time interval between the α cells is "long", there is a birth-order bias such that the first-born α cell always becomes the VU. When the birth-time interval between the α cells is "short," the decision is random with respect to relative birth order; instead, the first *parent* of an α cell (Z1.pp or Z4.aa) that expresses the transcription factor HLH-2 gives rise to the α cell that

becomes the VU. These two elements are inter-related because the relative order and timing of the first division of the precursors Z1 and Z4 are largely maintained throughout their lineages, so one parent is often born before the other; and the onset of HLH-2 expression begins within a narrow window after the birth of a parent cell, so if the birth-time interval is long, the first parent born will also express HLH-2 before the other parent does. However, when birth-time intervals are short, which parent expresses HLH-2 first is stochastic. A potential deterministic mechanism for the HLH-2 expression bias was suggested by the finding that HLH-2 is required for LIN-12 expression in the α cells. Thus, the recent model proposed that earlier expression of HLH-2 in a parent cell might give its α daughter an "edge" in LIN-12 activation, by promoting earlier *lin-12* transcription directly or indirectly, and therefore biasing it to be the αVU (Attner et al., 2019).

This model makes several predictions for the relationship between birth-time interval, relative birth-order, and LIN-12 activity (Figure 6A). These predictions could not be tested using LIN-12 target genes or nuclear localization of the intracellular domain because they are not visible early in the AC/VU decision, when the α cells are being influenced by stochastic events. The evidence described above suggests that SALSA is a faithful reporter of LIN-12 activity; in testing the predictions of the model, we would also be testing whether SALSA can perform as a rapid-response biosensor and reveal differences in signaling over time. We collected time-lapse spinning disk confocal videos of 58 worms with both the somatic gonad cleavable reporter and LIN-12::TEVp switch corresponding to 33 long and 25 short birth-time intervals (Figure S4 shows ten representative videos), and 16 individuals with only the somatic gonad cleavable reporter as a negative control. Under the imaging conditions used here and in Attner et al. (2019), a long birth-time interval corresponds to >45 minutes and a short birth-time interval, to ≤45 minutes (STAR Methods). By analyzing the level of LIN-12 activity in the α cells as a function of birth-time interval, and changes over time, we found evidence consistent with the recent model.

α cells do not differ in their initial level of LIN-12 activity.—Although endogenous LIN-12::GFP expression has not been detected in the parents of the α cells, endogenous GFP::HLH-2 and LAG-2::GFP have been observed (Attner et al., 2019). If there is a low level of LIN-12 activity in the parent cells, the first-born α cell may be born with an already-apparent advantage in LIN-12 activity. However, by quantifying the nuclear Red:Green between the first-and second-born α cells immediately after the birth of each cell, we ascertained that there is no significant difference in initial *lin-12* activity between the α cells regardless of birth-time interval, indicating that the birth-order bias for long birth-time intervals is not due to an inherent LIN-12 activity advantage in the first-born α cell at birth (Figure 6B). In addition, the parent cells do not appear to experience significant LIN-12 signaling (Figure S5), suggesting that differences in LIN-12 activity arise following the birth of the α cells.

When the birth-time interval is long, the first-born α cell gains a relative advantage in LIN-12 activity.—A fundamental prediction of the model is that for long birth-time intervals, the first-born α cell would experience significant LIN-12 signaling before the second-born α cell, and sustain an advantage over time, accounting for the

"edge." LAG-2 is detectable in the parents as well as in the α cells and their sisters, the β cells, when they are born (Attner et al., 2019). It is therefore conceivable that LIN-12 may be activated in the first-born α cell by ligand from its sister β cell and/or the undivided parent of the other α cell; alternatively, productive signaling may only occur between the two α cells and hence begins only after both have been born. In the former case, a long birth-time interval would give the first-born α cell a head-start in accumulating active LIN-12, a potential explanation for its bias towards VU fate. We quantified the level of LIN-12 activity in the first- and second-born α cells at the timepoint immediately following the birth of the second α cell (Figure 6C). This analysis revealed that the first-born α cell already has developed a significantly greater level of LIN-12 activity than the second-born α cell has at its birth when the birth-time interval is long, but not when the birth-time interval is short (Figure 6D).

***When the birth-time interval is short, the relative birth order does not predict which α cell will gain a relative advantage in* lin-12 *activity.*—**At short birth-time intervals, the α cell that adopts the VU fate is random with respect to birth order (Attner et al., 2019); we therefore tested whether the LIN-12 activity advantage is random as well (Figure 6E). We identified twelve animals with "short" birth-time intervals for which we could determine the relative birth order and observe the development of a clear difference in nuclear Red:Green ratio during the time period covered by the video (see STAR Methods for full details). The first-born α cell had a clear activity advantage in 6/12 cases and the second-born α cell had the advantage in the remaining 6/12 cases, demonstrating that when the birth-time interval is short, which α cell gains a LIN-12 activity advantage over the other is random with respect to birth order, as predicted by the model.

Discussion

SALSA as a tool for studying Notch signaling in vivo

We developed SALSA as a biosensor for live readouts of Notch activity and tested its efficacy in *C. elegans* for two different Notch proteins and in four different cell fate specification paradigms. In all cases, SALSA gave the anticipated readouts for Notch activity based on extensive prior genetic analysis and reporter gene studies. Our validation of SALSA in multiple paradigms provides optimism that it may be applied more generally to other systems.

We also successfully used SALSA for quantitative longitudinal imaging to test a recent model (Attner et al., 2019) for a simple lateral specification paradigm, the decision of two bipotential α cells between AC and VU precursor cell fates. In each individual worm, one α cell becomes the AC and the other becomes the αVU; however, each α cell has a 50% chance of being the AC. During the AC/VU decision, two stochastic elements are resolved into a deterministic mechanism: (1) the relative birth order, which reflects the timing of the division of the precursor three cell generations earlier, and (2) the onset of expression of the transcription factor HLH-2 in the parents of the α cells, which is linked to their birth. The model proposes that earlier HLH-2 expression in the parent cell gives its α daughter a

head start toward the onset of LIN-12 activation by ligand from neighboring cells so that it is biased to be the αVU (Attner et al., 2019).

Using SALSA, we corroborated three key predictions of the model. First, LIN-12 activity was not detected in the parent cells, and the first-born and second-born α cells had comparable levels of LIN-12 activity at their births, affirming that relevant LIN-12 activity occurs from signal transduction within the bipotential α cells themselves. Second, when the interval between the birth of the α cells was long, the first-born α cell gained a distinct advantage in LIN-12 activity before the second-born α cell was born and sustained that advantage over time. Third, when the interval between the birth of the α cells was short, the α cell that developed the LIN-12 activity advantage was random with respect to birth order. The success of SALSA in the AC/VU decision paradigm suggests that it will allow Notch responses to be studied as cell fate decisions progress in other lateral signaling paradigms.

Other potential applications of SALSA for studies of Notch signaling in vivo or ex vivo, and for further customizing SynNotch responses

We suggest here other potential applications, and the modularity of switch and reporter design (Figure 7) should allow others to be devised.

i. SALSA may be incorporated into cell-based assays or organoids ex vivo in situations where its design features may offer advantages over other methods.

ii. For noncanonical Notch signaling mechanisms, transcription of targets of the canonical pathway are not useful reporters of signaling (Hunter and Giniger, 2020). Thus, SALSA offers an approach to assessing noncanonical Notch signaling mechanisms that involve cleavage, such as regulation of the cytoskeleton by suppression of Abl activity in the growth cone that occurs during axon guidance in Drosophila (Kannan et al., 2018). The switch or the reporter design may be varied (Figure 7) to facilitate detection of activity if the intracellular domain does not gain sufficient access to the nucleus during these noncanonical signaling events.

iii. SALSA may help identify as-yet unknown cell contexts where Notch is active, independent of potential context-dependent effects on transcriptional reporters of signaling activity. This potential application may be particularly valuable for reporting activation of individual Notch paralogs when there is functional redundancy, as has been seen in *C. elegans* and mammals (Krebs et al., 2000; Lambie and Kimble, 1991; de la Pompa et al., 1997). It may also be valuable when pleiotropic effects from Notch pathway mutants such as embryonic lethality precludes easy assessment of the contribution of Notch signaling to later developmental events or by lineage-marking strategies.

iv. ”SynNotch” proteins incorporate the force-sensing negative regulatory region of Notch into chimeric receptors that contain a heterologous recognition domain in the ectodomain and a heterologous transcription factor as the intracellular domain. This arrangement allows for the creation of a customized signal-response system in which a ligand causes cleavage and release of a tethered

transcription factor (Ho and Morsut, 2021; Morsut et al., 2016), and its practical applications include anti-cancer therapy by engineered chimeric antigen receptor T cells (Cho et al., 2018; Choe et al., 2021; Hyrenius-Wittsten et al., 2021; Roybal et al., 2016; Srivastava et al., 2019). We envisage that a SynNotch modeled on our Notch::TEVp switch, combined with different reporters modeled on our nuclear-tethered GFP (Figure 7), could be used to expand the range of "SynNotch"-type applications in artificial circuits to processes other than transcription. For example, ligand-mediated release and translocation of TEVp to the nucleus could release a nuclear-tethered protein to function in the cytosol, or convert a nucleartethered pro-protein into an active protein via cleavage of a Tcut site. This type of activation would allow for immediate, amplified production of active protein without the caveats of a transcriptional activation step.

Limitations of SALSA

Our analysis suggests that SALSA is sensitive to the onset of signal transduction, and the increase in the nuclear Red:Green ratio over time as the α cells interact via LIN-12/Notch suggests that it is a good proxy for the cumulative level of signaling they experience, fulfilling our aims for studying how stochastic differences affect signaling in the initial stages of the AC/VU decision. However, for some quantitative applications, it may be valuable to characterize a dose-response relationship by systematically varying the ligand concentration; it may also be valuable to characterize how rapidly the nuclear Red:Green ratio (or Cytoplasmic:Nuclear Green ratio) returns to baseline after ligand is initially present but then withdrawn. These tests were not feasible in our analysis, as we relied on natural ligand expression, and could only perform a simple presence-or-absence ligand comparison (as we did in the M lineage and VPCs). The correlation of activity based on GLP-1/Notch SALSA in the germ line with known target gene expression patterns suggests that SALSA will perform well in such tests, since the distance from the DTC represents a temporal progression from a region of high signaling to a region of low signaling, a gradient which has been proposed to be determined in part by decreasing levels of interaction with ligand expressed by the DTC as cells moves proximally (Lee et al., 2016).

The question about the "off rate" is pertinent to the potential suitability of SALSA for studying modulation of properties such as frequency, amplitude and duration of signal transduction, which have been demonstrated to cause different outcomes for some signaling pathways (Albeck et al., 2013; Atay and Skotheim, 2017; Johnson and Toettcher, 2019; Purvis and Lahav, 2013; Ryu et al., 2015). For Notch, little is known about whether such properties are modulated during signaling. The main evidence to date for such modulation comes from a study of responses to different mouse ligands ex vivo (Nandagopal et al., 2018). This study reported that a ligand with low affinity for Notch causes pulsatile cleavage and a ligand with high affinity causes more sustained cleavage, correlated with expression of different Notch target genes. However, the study did not exclude the possibility that the relevant parameter is the absolute level of signaling and not the dynamics; indeed, it has been proposed that the different transcriptional profiles may instead be explained by feedback circuits elicited by different levels of signal transduction (Henrique and Schweisguth, 2019). Such robust feedback mechanisms are characteristic of diverse Notch-

mediated cell fate decisions in vivo, such as the generation of spaced bristle patterns in Drosophila (Corson et al., 2017; Couturier et al., 2019; Heitzler et al., 1996), reiterated somite formation in vertebrates (Diaz-Cuadros et al., 2021; Hubaud and Pourquié, 2014; Hubaud et al., 2017), and the AC/VU decision (Greenwald, 2012). Furthermore, there is also evidence in Drosophila that in individual cells, the cumulative amount of Notch activation is what governs expression of a key target gene during development (Falo-Sanjuan et al., 2019; Viswanathan et al., 2019), consistent with the view of LIN-12/Notch activity as a binary switch driven by feedback amplification of stochastic initial differences during the AC/VU decision and the measurements of signal transduction described here.

As with any biosensor system, an intrinsic limitation of SALSA is the requirement to optimize the levels of expression as well as other properties of the interacting components to detect biologically meaningful responses *in vivo*. We used Notch::TEVp knock-in alleles to achieve physiological levels of expression and activity of the switch, and single-copy insertion transgenes driving uniform expression of cleavable reporters at levels we could easily visualize and quantify. Our characterization indicated that these conditions were appropriate for our experimental goals. However, for implementing SALSA in other experimental systems, some of these details may need to be varied, and for some applications, it may also be necessary to assess the performance of SALSA further; for example, if genetic backgrounds that are known to sensitize for perturbations in Notch activity are going to be used for the study, then it may be necessary to test if the tagged alleles behave like wild-type alleles in the relevant backgrounds.

For analysis, we used the nuclear Red:Green ratio to quantify activity, and as described herein, our analysis suggests it was accurate for our applications. However, a ratiometric measurement using a “cytoring” to calculate a Green Cytoplasmic:Nuclear (C:N) fluorescence ratio (Regot et al., 2014) of free GFP after reporter cleavage may be more accurate or more sensitive if the two fluorescent proteins have different half-lives or photobleaching rates, although the cells must be large and spaced enough to allow for good segmentation. Both the nuclear Red:Green and Green C:N ratiometric measurements have the virtue that they internally control for differences in expression level of the reporter in different cells.

Finally, we note that modifications to the cleavable reporter, such as adding a degron to one of the fluorescent proteins or changing the nuclear localization signal in the cleavable reporter from a histone to an NLS, may alter the sensitivity or resolution of the system. Moreover, a cleavable reporter may be engineered to make measurements based on relieving FRET instead of a change in nucleocytoplasmic localization. The modular nature of SALSA and the large number of modifiable parameters offer many potential ways to optimize it for other systems and purposes.

STAR Methods

RESOURCE AVAILABILITY

Lead contact—Further information and requests for resources and reagents should be directed to and will be fulfilled by the Lead Contact, Iva Greenwald (isg4@columbia.edu).

Materials Availability—All materials are available upon request.

Data and code availability—All data reported in this paper will be shared by the lead contact upon request.

This paper does not report original code.

Any additional information required to reanalyze the data reported in this paper is available from the lead contact upon request.

EXPERIMENTAL MODEL AND SUBJECT DETAILS

***C. elegans* alleles and transgenes—**C. elegans strains were maintained at 20°C on 6 cm NGM plates seeded with E. coli OP-50. See the Key Resources Table for full list of strains. All experiments were performed at 25°C to maximize fluorescent reporter intensity.

Details of the generation of all alleles are outlined in the Method Details section. The alleles *lin-12(ar640)* and *glp-1(ar648)*, which encode for the LIN-12::TEVp and GLP-1::TEVp switches, respectively, were generated using CRISPR/Cas9 to tag the endogenous loci at the C terminus with TEV protease.

The transgenes *arTi355, arTi351*, *arTi359*, and *arTi356* were made using miniMos transposons (Frøkjær-Jensen et al., 2014) to generate single copy genomic insertions, described in Method Details.

arTi237[ckb-3p::Cre(opti)] is a miniMos-based transgene, made as described in (Tenen and Greenwald, 2019) and found in strain GS8795, that expresses Cre recombinase optimized for use in *C. elegans* (Ruijtenberg and van den Heuvel, 2015) in the developing somatic gonad. The *ckb-3p* sequence drives expression in Z1 and Z4 beginning in the embryo (Kroetz and Zarkower, 2015) and results in highly efficient excision of the *flexon* cassette of the SALSA reporter *arTi355[rps-27p::gfp(flexon)::tcut::mScarlet::h2b]*, resulting in strong, tissue specific expression of the cleavable reporter in all somatic gonad cells. The Flexon approach is described in Shaffer and Greenwald (2022).

hlh-2(ar614), described in (Attner et al., 2019) contains a deletion of a regulatory element that eliminates HLH-2 expression only in Z1.pp, Z4.aa, and their daughter cells. Because *hlh-2* activity in these cells is necessary for an AC to be specified (Karp and Greenwald, 2003; 2004; Sallee and Greenwald, 2015), this mutant lacks an AC. Thus, P6.p is not induced to express the lateral signal that activates LIN-12/Notch in P5.p and P7.p. Because both the EGF-like and lateral signals are missing, the daughters of the VPCs fuse to the major hypodermal syncytium.

The strains GS9324, GS9399, and GS9317 were generated directly through injection and transgenesis, as described in Method Details. The strains GS9215, GS9338, GS9854, GS9339, GS9452, GS9447, GS9322, and GS9314 were generated through crosses and checked for homozygosity by genotyping PCR.

METHOD DETAILS

Generating *Notch::TEVp alleles*—We used the self-excising cassette (SEC) method to generate *lin-12(ar640)[lin-12::tevp]* (Dickinson et al., 2015). The repair template pJS106 was made in a two-step Gibson cloning process (Gibson et al., 2009; NEB Inc. E2621) in which (1) an intermediate plasmid pJS87 was generated by replacing the GFP and tev cut site sequences of a pBluescript based SEC vector pJC41 with a 2.1 kb 5' homology arm for the *lin-12* locus, and (2) the coding sequence for TEV protease (Barnea et al., 2008) and a 1.6 kb 3' homology arm for the *lin-12* locus were added.

To generate the *lin-12(ar640)* allele, we injected the repair template pJS106 (50 ng/μl), two *lin-12* directed sgRNA and Cas9 expressing plasmids pJC54 and pJC55 (25ng/μl each), and the co-injection markers pCFJ90 (7.5 ng/μl) and pGH8 (10 ng/μl) into the germline of GS8949 *hlh-2(ar623)[gfp::tcut::hlh-2]* hermaphrodites. The injected hermaphrodites were placed at 25°C, and treated with hygromycin after 3 days to select for integrants. Progeny with a roller (Rol) phenotype were picked 7 days post-injection, and checked for homozygosity. The SEC was then excised by heat shocking at 32° for 4 hours and picking non-Rol progeny. The *lin-12(ar640)* allele was then isolated by standard crossing to generate the strain GS9215.

To generate *glp-1(ar648)[glp-1::tevp]*, we used a *dpy-5* co-CRISPR strategy (Kim et al., 2014). The repair template pJS135 was made using Gibson cloning to insert fragments containing a 676 bp 5' homology arm for the *glp-1* locus, the coding sequence for TEVp, and a 661 bp 3' homology arm for the *glp-1* locus into a pBlueScript (KS)+ vector backbone. The sgRNA and Cas9 expressing plasmids pJS131 and pJS132 were generated using Gibson cloning to replace the *pha-1* targeting sequence in pJW1285 (Ward, 2015) with sequences targeting the *glp-1* locus.

To generate the *glp-1(ar648[glp-1::tevp])* allele, we injected the repair template plasmid pJS135 (50 ng/μl), the *glp-1* directed sgRNA and Cas9 expressing plasmids pJS131 and pJS135 (25 ng/μl each), and a *dpy-5* directed sgRNA and Cas9 expressing plasmid pDR91 (gift from Abhishek Bhattacharya) into N2 hermaphrodites. Injected animals were placed at 25°C. Dpy progeny were isolated 4 days post-injection and allowed to lay eggs for 1 day prior to lysis and PCR to check that the sequence was inserted.

Phenotypic analysis of *Notch::tevp alleles*—*lin-12(ar640)* and *glp-1(ar648)* hermaphrodites appear indistinguishable from wild-type hermaphrodites, in that we observed no apparent defects in egg-laying or fecundity that might indicate compromised Notch activity during the course of maintaining and working with strains containing these alleles. Nevertheless, to support this inference, we examined GS9314 *lin-12(ar640) [lin-12::tevp]; somatic gonad cleavable reporter* and GS9447 *arSi85[mex-5p::reporter]; glp-1(ar648)[glp-1::tevp]* hermaphrodites more closely.

To verify that GS9314 does not have defects associated with compromised *lin-12* function, we examined hallmark cell fate decisions in gonadal and vulval development analyzed in Figures 2, 5, and 6. We allowed 13 adult GS9314 hermaphrodites to lay eggs for 2 hours on one plate and then examined the progeny in mid-L4 for the number of ACs and

vulval morphology; all (100%) had 1 AC and wild-type vulval morphology (n=41). We also examined late L4 for uterine-seam (utse) cell formation, which requires *lin-12*-mediated cell fate decisions in VU descendants (Newman et al., 1995); all (100%) had proper utse formation (n=25). Furthermore, we examined GS9314 hermaphrodites for egg-laying defects, which, in addition to normal vulval and uterine development, requires proper *lin-12* function during sex muscle differentiation (Foehr and Liu, 2008; Hale et al., 2014; Li et al., 2013): we picked 50 GS9314 L4 larvae to individual plates and verified that all were able to lay eggs normally.

To verify that *glp-1(ar648)* does not cause defects associated with compromised *glp-1* activity, we performed two assessments. Maternal *glp-1* is required early in embryogenesis; *glp-1(−)* mutations cause embryonic lethality in the progeny (Austin and Kimble, 1987; Priess et al., 1987). To test for embryonic viability, we examined progeny of ten GS9447 *arSi85[mex-5p::reporter]; glp-1(ar648)[glp-1::tevp]* and nine N2 wild-type hermaphrodites: we placed individual L4 larvae on separate plates, removed the hermaphrodites the next day, and scored for dead eggs after allowing the progeny to hatch overnight. There were five total dead eggs on ten plates total for GS9447 and four dead eggs on nine total plates for N2, suggesting that *glp-1(ar648)* function is wild-type during embryogenesis. In addition, as hypomorphic mutations in *glp-1* can reduce brood size due to the combination of embryonic lethality and reduced germline stem cell maintenance (Austin and Kimble, 1987), we counted total broods for three L4 larvae of GS9447 and N2, passing them every day onto fresh plates, and counting the number of progeny on each plate about 24 hours after passage. We found that GS9447 (n=244, 223, 195; average=220.7) and N2 (n=242, 236, 179; average=219.0) animals produced similar levels of progeny, and the number expected for wild-type worms raised at 25° (Byerly et al., 1976), indicating that *glp-1(648)* functioned indistinguishably from *glp-1(+)*.

Reporters

The cleavable reporters presented in this study use diffusion of GFP out of nucleus after cleavage from a nuclear RFP::H2B tether by TEV protease as a readout for LIN-12 activity. The GFP sequence is from pDD282 (Dickinson et al., 2015) and is codon-optimized for *C. elegans*. The mScarlet sequence is also codon optimized for *C. elegans* (wrmScarlet; El Mouridi et al., 2017) with a synthetic intron added for efficient expression; the H2B sequence is from *his-58*. The reporters used in Figure S1 and 4 use mCherry::H2B instead of mScarlet::H2B, but all other components are identical. A 51 bp linker sequence between the GFP and RFP sequences (GAGAATCTGTACTTTCAATCCGGAAAGGGAGGTGGATCCGGAGCCGGATCT) encodes the 7 amino acid residue long TEV recognition site (ENLYFQS) and a 10 residue long flexible linker sequence (GKGGGSGAGS). Under our imaging conditions, we did not detect any FRET between the two fluorescent proteins in the cleavable reporter, or photoconversion of mScarlet, as described below in Still imaging in the M lineage, VPCs, germline, and somatic gonad.

We also tested cleavable reporters that added a nuclear export signal (NES) tag onto GFP: NES sequences from HIV-1 Rev, human MAP2K2, *C. elegans* MEK-2, and human

RANBP1 (Xu et al., 2012). All of the NES sequences facilitated the nuclear export of free GFP in cells with reporter cleavage, but they all also caused uncleaved reporter to localize to the cytoplasm, thus obscuring segmentation and reducing the overall dynamic range of the system. The extent of ectopic cytoplasmic localization varied by cell type, so it remains possible that an NES sequence may improve reporter performance in other tissues and systems.

VPC cleavable reporters: The 5' regulatory region for the VPC cleavable reporters consist of the 5' and intronic sequences from *lin-31*, called *lin-31p* (Tan et al., 1998). *arTi351[lin-31p::gfp::tcut::mScarlet::h2b]* was made using plasmid pJS119, and *arTi356 [lin-31p::gfp::tcut::mCherry::h2b]* was made using plasmid pJ128. Both plasmids were cloned using Gibson assembly to insert the respective coding regions into pCC249, a miniMos vector with the *lin-31p* regulatory sequence.

M lineage cleavable reporter: The 5' regulatory region of the M lineage cleavable reporter consists of sequences from the 5' region of *hlh-8*, called *hlh-8p* (Harfe et al., 1998). *arTi359[hlh-8p::gfp::tcut::mScarlet::h2b]* was made using pJS136, which was made by restriction cloning with *Age*I-HF and *Bgl*II to insert *gfp::tcut::mScarlet* from pJS119 into the miniMos vector pJS107 that contained *hlh-8p* and *h2b*. The transgene was generated in the *lin-12(ar640)* background and fortuitously inserted at a site tightly linked to *lin-12*, and was not separated for analysis on its own.

Somatic gonad cleavable reporter: *arTi355[rps-27p::gfp(flexon)::tcut::mScarlet::h2b*] was made using plasmid pJS126, which was cloned using Gibson assembly to insert the gene region into the blank miniMos vector pCFJ910. The *flexon* is flanked by *lox2272* sites so as not to recombine with the *loxP* site present in the *lin-12(ar640)* switch which was generated during the course of engineering that allele using the method (Dickinson et al., 2015).

Standard protocols for isolating and mapping single copy insertions from miniMos vectors were used to generate each of the above transgenes from their respective plasmids (Frøkjær-Jensen et al., 2014; wormbuilder.org). Young adult hermaphrodites were injected with a solution containing the vector plasmid (10 ng/μl), the Mos transposase-containing plasmid pCFJ601 (50 ng/μl), the heat shock-induced negative selection plasmid pMA122 (10ng/μl), and the co-injection markers pGH8 (10 ng/μl) and pCFJ90 (2.5 ng/μl). After injection, plates were placed at 25°. 250 μl of 25 mg/ml G418 was added to the plates 2–3 days after injection, and then the plates were left to starve. About 7–10 days after injection, plates that starved out and had lost co-injection marker expression were subjected to a 2 hour heat shock at 34°, and then plates were chunked the next day onto plates containing G418. After another day, individuals that appeared healthy were isolated; the transgene was mapped in their progeny by inverse PCR and then homozygosed by genotyping PCR.

Germline cleavable reporter: The 5' regulatory region for the germline cleavable reporter contains 5' sequences from *mex-5*, called *mex-5p*; the 3' UTR from *tbb-2* was used for germline permissibility (Merritt et al., 2008). *arSi85[mex-5p::gfp::tcut::mCherry::h2b:tbb-2 3' UTR]* was generated using the SEC

method to insert a single-copy transgene into a locus (*ttTi4348*) that is permissive to germline and early embryonic expression (Frøkjær-Jensen et al., 2012). The repair template pJS134 was made using Gibson cloning to insert *gfp::tcut::mCherry::h2b* into the SEC vector pCC357 (de la Cova et al., 2017), which contains homology arms for the *ttTi4348* locus and the sequences for *mex-5p* and *tbb-2 3' UTR*. To generate *arSi85*, adult N2 hermaphrodites were injected with the repair template pJS134 (50ng/μl), the Cas9 and *ttTi4348* targeting sgRNA expressing plasmid pAP582 (50 ng/μl; Pani and Goldstein, 2018), and the coinjection markers pGH8 (10 ng/μl) and pCFJ90 (2.5 ng/μl). The allele was isolated following the protocol outlined above in the generation of *lin-12(ar640)*.

Still imaging

Animals were imaged using a Zeiss AxioObserver Z1 inverted microscope with a 63X, 1.4NA oil immersion objective and a spinning disk. A 488 nm, 100mW laser was used to excite GFP and a 561 nm, 75 mW laser was used to excite the RFPs. Z-stacks of GFP and RFP fluorescence were simultaneously captured with a dual-camera system.

When indicated, timed egg-lays were performed for developmental synchronization. Gravid hermaphrodites were placed on a seeded plate and allowed to lay eggs for 1 hour before removal, and progeny were allowed to grow until the desired developmental stage was reached.

VPCs (Figure 2B, S1): For GS9338 *lin-12(ar640)[lin-12::tevp]; arTi351[lin-31::reporter]* and GS9324 *arTi351*, larvae were incubated for approximately 30 hours after egglay prior to imaging. Since GS9854 *hlh-2(ar614); lin-12(ar640); arTi351* do not have vulvae and do not lay eggs, animals were synchronized using a standard bleaching protocol (Stiernagle, 2006) to isolate embryos; hatched larvae were collected three hours after bleaching and incubated prior to imaging for about 22 hours. For imaging, larvae for each genotype were mounted onto a 3% agarose pad and immobilized with 10 mM levamisole. The following parameters were used for imaging: 250 ms exposure in both channels, 400 EM gain, 3% GFP 488 nm laser power, 25% 561 nm laser power, and 600 nm slice intervals. The same egglay conditions, preparations, and imaging parameters were used for GS9339 *arTi356[lin-31::reporter]; lin-12(ar640)* and GS9452 *arTi356; lin-12(ar640); sel-10(ar41).* GS9452 also contains transgenes for fluorescent somatic gonad markers that do not interfere with segmentation or quantitation of the VPCs (Key Resource Table).

M lineage (Figure 3,S3): Approximately 17 hours after egg lay, GS9399 *arTi359[hlh-8p::reporter] lin-12(ar640)[lin-12::tevp]* larvae were mounted onto a 3% agarose pad and immobilized with 10 mM levamisole. The following parameters were used for imaging: 250 ms exposure in both channels, 400 EM gain, 15% GFP 488 nm laser power, 30% 561 nm laser power, and 600 nm slice intervals.

Germ line (Figure 4): L4 larvae from unsynchronized plates of either GS9447 *arSi85[mex-5p::reporter]; glp-1(ar648)[glp-1::tevp]* or GS9317 *arSi85* were mounted onto a 3% agarose pad and immobilized with 10 mM levamisole. The following parameters were

used for imaging: 250 ms exposure in both channels, 400 EM gain, 4% GFP 488 nm laser power, 25% 561 nm laser power, and 1 μm slice intervals.

Specified AC and VU (Figure 5): GS9314 *lin-12(ar640)[lin-12::tevp]; somatic gonad cleavable reporter* or control GS9322 *somatic gonad cleavable reporter* larvae were picked from unsynchronized plates, mounted onto a 3% agarose pad and immobilized with 10 mM levamisole. Late L2/early L3 larvae were selected for imaging based on gonad size and morphology. The following imaging parameters were used: 150 ms exposure in both channels, 400 EM gain, 4% GFP 488 nm laser power, 25% 561 nm laser power, and 600 nm slice intervals.

To test for FRET activity, GS9322 *somatic gonad cleavable reporter* animals were imaged using identical conditions to those outlined above, but with 0% 561 nm laser power; the photomicrographs were then inspected for red fluorescence. The somatic gonad cleavable reporter was used for assessing FRET because the Flexon system produces the brightest reporter expression of all strains used; if there was FRET activity, it would be the most evident with this reporter. However, there was no observable red fluorescent emission under these imaging conditions.

To test for mScarlet photoconversion from red to green emission under simulated time-lapse imaging conditions, GS9770 *arTi430[rps-27p::mScarlet(flexon)::h2b::unc-54 3'UTR]; arTi237[ckb-3p::cre(opti)]* [gift of Jee Hun (Henry) Kim] were prepared for imaging as described above and then illuminated with the 561 nm laser at 25% power for 10 minutes prior to imaging with identical parameters to the what was used for time-lapse imaging. No green spectrum fluorescence was observed after the extended illumination.

Time-Lapse Imaging

We note that the use of confocal imaging required keeping worms anesthetized, limiting the length of the videos we could take of young larvae without introducing complications from starvation or the inability to molt. The microfluidic device used previously for high-throughput lineage analysis of the AC/VU decision is not compatible with confocal microscopy (Keil et al., 2017; Attner et al., 2019). The possibility of microfluidic devices compatible with confocal microscopy may allow for longer-term imaging of SALSA in *C. elegans* (Berger et al., 2021). These constraints would not necessarily apply to other ex vivo (e.g. Hung et al., 2017; Regot et al., 2014; Ryu et al., 2015) or in vivo (Johnson and Toettcher, 2019; Pokrass et al., 2020; Simon et al., 2020) systems.

M lineage (Figure S3): GS9399 L1 larvae were picked from an asynchronous plate into 48 ul of 0.1% tricaine/0.01% tetramisole in M9 and incubated at room temperature for 30 minutes. Anesthetized larvae were then mounted into 0.01% tricaine/0.001% tetramisole in M9 on a 4% agarose pad. Animals in the 2-M stage were selected for movies. Imaging was performed using spinning disk microscopy, with the following parameters: 250 ms exposure for both channels, 800 EM gain, 3% 488 nm laser power, 25% 561 nm laser power, and 600nm slice intervals. Z stacks for up to 6 larvae per pad were taken at 15 minute intervals for 25 timepoints, which does not compromise larval development.

Somatic Gonad (Figure 6, S4): GS9314 and GS9322 animals were synchronized with egg lays in which 15 gravid hermaphrodites were allowed to lay eggs on a plate for 1 hour followed by removal of the adults. The plate was then incubated at 25°C for 21–21.5 hours to begin imaging in mid L1. Larvae were mounted and anesthetized using the same protocol as outlined for the M lineage movies. Larvae were selected for imaging by the extent of gonad progression (undivided Z1.pp and/or Z4.aa).

Imaging was performed using spinning disk confocal microscope setup described above, to produce images allowing for accurate ratiometric quantification. The larvae are viable for approximately 6 hours under these conditions, allowing for capture of the birth-time interval and birth order, but not the final cell fate, which was inferred based on earlier studies (Attner et al., 2019). Imaging parameters were the same as for the M lineage movies, except with 150 ms exposure for both fluorescent channels.

Image quantification

Images for the M lineage (Figure 3C,D), and the somatic gonad (Figures 5,6,S5), were processed and quantified using published protocol, workflow, and code (de la Cova et al., 2017; Luo et al., 2020). In summary, after illumination correction, the red fluorescence intensity value was divided by the green fluorescence intensity value for each pixel of every slice, and then normalized between 0.1 and 99.9% to avoid pixel artifacts. Segmentation by red fluorescence and quantitation was performed with Cellprofiler (Kamentsky et al., 2011). Tracking the nuclei was done using Matlab scripts from de la Cova et al. (2017) with the leniency parameter increased from 5 to 10 to accommodate for increased worm movement during time-lapse imaging, and extraction of the average upper quartile intensity of the three most equatorial slices for each nuclei of interest was performed using Matlab scripts adapted from Luo et al. (2020). For the time-lapse imaging in the somatic gonad, the “method to draw dividing lines between clumped objects” parameter in the CellProfiler pipeline module “IdentifyPrimaryObjects” was changed to *shape* to draw borders between close nuclei based on shape instead of intensity.

For quantifying the VPCs (Figure 2B,S1), prior to entering the pipeline the GFP and red channels were aligned using auto channel alignment in Zen for translational and rotational alignment, with the red channel as reference and using the highest quality setting. This prevented us from using the Red:Green pixel values, so Matlab scripts adapted from Luo et al. (2020) were used extract the average nuclear red and green fluorescence intensities for the three equatorial slices and divide the average red by the average green values to create a nuclear Red:Green ratio.

For testing different quantitation methods using the M lineage (Figure S2), the channels were aligned as described above. The original pipeline was altered to define the cytoring in the following way. After primary object identification and segmentation of a “prenucleus,” the edges of each object were expanded by 1 pixel to form a “postnucleus,” and then a secondary object was identified by expanding the postnucleus by 5 pixels; the area between the outer ring and the postnucleus was called the cytoring. The cytoring was used as the cytoplasmic measurement because it was difficult to distinguish cell borders *in vivo* in multilayered, complex tissues without an additional membrane marker which would affect

segmentation. Using this pipeline, we extracted the values for average nuclear Red:Green, nuclear 1/Green, and Cytoring:Nuclear Green fluorescence for the three equatorial slices of each cell as described above, and compared them to each other and to the original nuclear pixel Red:Green values used in Figure 3C.

For quantifying the germ line (Figure 4), images of the germ line of L4 larvae were first aligned using Zen's channel alignment tool as described above. There were too many nuclei in too many planes in each image for effective segmentation using our pipeline, so nuclei were manually segmented using ImageJ to draw circles around the nuclei of interest. Nuclei were selected for quantification according to distance in microns from the distal end using the conversion of 3.5 microns per cell diameter, which is approximately the average of previously used conversion metrics (Chen et al., 2020; Lee et al., 2019). Three nuclei per position (0, 5, 10, 15 cd) were quantified for each germline arm. The equatorial three slices of each nuclei were found based on the integrated density of red fluorescence, and the average nuclear Red:Green integrated density per slice was averaged across the three equatorial slices for each nuclei. .

We note that we needed to use different methods and imaging parameters to generate the nuclear Red:Green ratios in each context, resulting in differences in the measurement scales in the graphs shown in the figures. However, we present internal controls for each tissue context for which all parameters and measurements methods were identical.

QUANTIFICATION AND STATISTICAL ANALYSIS

All statistical analysis was performed in GraphPad Prism. The minimum level of significance for all analysis was set at 0.05 prior to corrections for multiple testing. Every data set was subjected to D'Agostino & Pearson tests of normality before proceeding with the appropriate statistical tests. To compare nuclear Red:Green ratios of VPCs within genotypes (Figure 2), we performed a repeated measures ANOVA with Greenhouse-Geisser correction, and post hoc comparisons using the Tukey HSD test for every possible pairwise comparison for each genotype. To compare nuclear Red:Green ratios between genotypes in the VPCs (Figure 2) and in the germline (Figure 4), we performed ordinary one-way ANOVA tests and post hoc comparisons using Tukey HSD tests for every possible pairwise comparison. For comparing nuclear Red:Green fluorescence in *sel-10(+)* and *sel-10(−)* animals (Figure S1), we performed an ordinary one-way ANOVA, and post hoc comparisons with Bonferroni corrections to compare each VPC between the two genotypes. When comparing SALSA activity in dorsal and ventral cells in the M lineage, we performed an unpaired t-test (Figures 3C,S1), and a one sample t-test was used to compare the difference in nuclear Red:Green between the dorsal and ventral cells within every worm to the expected mean of zero (Figure 3D). To compare nuclear Red:Green between the αVU and the AC in L3 (Figure 5), we performed paired t-tests. To compare the differences in nuclear Red:Green between alpha cells (Figure 6) and parent cells (Figure S5) for different birth-time intervals, we used a Kruskal-Wallis H test with post hoc comparisons using Dunn's correction for every possible pairwise comparison within each test.

The imaging conditions we used here, with fluorescence images captured every 15 minutes, were comparable to those used in Attner et al. (2019), where the cut-off between "long"

and “short” birth orders were established according to cell fate outcome. Assessing outcome in that study was possible because it utilized a microfluidic device. In this study, we could not observe the final fate outcomes of the cells imaged in the short-term imaging conditions we had to use to allow for confocal microscopy, so in addition to using the bins established previously, we performed an independent statistical analysis of our data to determine the cutoff between short and long birth-time intervals under these conditions. We binned animals into “short” or “long” birth-time intervals based on whether the α cells were born less than or greater than a specific time interval apart. We used Mann-Whitney tests to compare the nuclear Red:Green differences between alpha cells within every worm for “short” vs. “long” birth-time intervals, beginning with a 30 minute birth-time interval cutoff and increasing the time interval stepwise. The most statistical significance was generated when the “short” bin included birth-time intervals ≤45 minutes, and the “long” bin included birth-time intervals >45 minutes; therefore, we considered α cell pairs with ≤45 minute birth-time intervals to be “short”, and α cell pairs with >45 minute birth-time intervals to be “long”. These bins are consistent with those used in (Attner et al., 2019).

For short birth-time intervals, we considered an α cell to have developed an advantage in LIN-12 activity if it had a higher nuclear Red:Green ratio than the other α cell for at least three successive timepoints, or a difference in nuclear Red:Green ratio of >0.1 units, at the end of the video or last comparable time point.

Supplementary Material

Refer to Web version on PubMed Central for supplementary material.

Acknowledgements

We gratefully acknowledge Michelle Attner for suggesting the use of TEVp and additional discussion throughout this project. We also thank Claire de la Cova for much helpful advice on statistical analysis, Tim Schedl for discussion about the germ line, Ruben Gonzalez and Colin Kinz-Thompson for advice on testing for FRET, and Michelle Attner, Catherine O’Keeffe, Gary Struhl and Sergi Regot for insightful comments on the manuscript. This work was supported by R35GM131746 from the National Institute of General Medical Sciences (to I.G.), and F31EY030331 from the National Eye Institute (to J.M.S.). J.M.S. was also supported by training grant T32GM008798. Some strains used during the course of genetic manipulations were provided by the CGC, which is funded by NIH Office of Research Infrastructure Programs (P40 OD010440).

References

Albeck John G., Mills Gordon B., and Brugge Joan S. (2013). Frequency-Modulated Pulses of ERK Activity Transmit Quantitative Proliferation Signals. Molecular Cell 49, 249–261. [PubMed: 23219535]

Atay O, and Skotheim JM (2017). Spatial and temporal signal processing and decision making by MAPK pathways. Journal of Cell Biology 216, 317–330. [PubMed: 28043970]

Attner MA, Keil W, Benavidez JM, and Greenwald I.(2019). HLH-2/E2A Expression Links Stochastic and Deterministic Elements of a Cell Fate Decision during *C. elegans* Gonadogenesis. Current Biology 29, 3094–3100.e3094. [PubMed: 31402303]

Austin J, and Kimble J.(1987). *glp-1* is required in the germ line for regulation of the decision between mitosis and meiosis in C. elegans. Cell 51, 589–599. [PubMed: 3677168]

Barnea G, Strapps W, Herrada G, Berman Y, Ong J, Kloss B, Axel R, and Lee KJ (2008). The genetic design of signaling cascades to record receptor activation. Proceedings of the National Academy of Sciences of the United States of America 105, 64–69. [PubMed: 18165312]

Berger S, Spiri S, deMello A, and Hajnal A.(2021). Microfluidic-based imaging of complete C. elegans larval development. Development (Cambridge, England).

Berry LW., Westlund B., and Schedl T. (1997). Germ-line tumor formation caused by activation of glp-1, a Caenorhabditis elegans member of the Notch family of receptors. Development (Cambridge, England) 124, 925–936.

Berset T, Hoier EF, Battu G, Canevascini S, and Hajnal A.(2001). Notch Inhibition of RAS Signaling Through MAP Kinase Phosphatase LIP-1 During *C. elegans* Vulval Development. Science (New York, NY) 291, 1055–1058.

Bothma JP, Norstad MR, Alamos S, and Garcia HG (2018). LlamaTags: A Versatile Tool to Image Transcription Factor Dynamics in Live Embryos. Cell 173, 1810–1822.e1816. [PubMed: 29754814]

Byerly L, Cassada RC, and Russell RL (1976). The life cycle of the nematode Caenorhabditis elegans: I. Wild-type growth and reproduction. Developmental biology 51, 23–33. [PubMed: 988845]

Chan J.(2020). Investigations into roles for endocytosis in LIN-12/Notch signaling and its regulation. In Biological Sciences (Columbia University).

Chen J, Mohammad A, Pazdernik N, Huang H, Bowman B, Tycksen E, and Schedl T.(2020). GLP-1 Notch—LAG-1 CSL control of the germline stem cell fate is mediated by transcriptional targets lst-1 and sygl-1. PLOS Genetics 16, e1008650.

Cho JH, Collins JJ, and Wong WW (2018). Universal Chimeric Antigen Receptors for Multiplexed and Logical Control of T Cell Responses. Cell 173, 1426–1438.e1411. [PubMed: 29706540]

Choe JH, Watchmaker PB, Simic MS, Gilbert RD, Li AW, Krasnow NA, Downey KM, Yu W, Carrera DA, Celli A, et al. (2021). SynNotch-CAR T cells overcome challenges of specificity, heterogeneity, and persistence in treating glioblastoma. Science Translational Medicine 13, eabe7378.

Corson F, Couturier L, Rouault H, Mazouni K, and Schweisguth F.(2017). Self-organized Notch dynamics generate stereotyped sensory organ patterns in *Drosophila*. Science (New York, NY) 356, eaai7407.

Couturier L, Mazouni K, Corson F, and Schweisguth F.(2019). Regulation of Notch output dynamics via specific E(spl)-HLH factors during bristle patterning in Drosophila. Nature Communications 10, 3486.

Crittenden SL, Troemel ER, Evans TC, and Kimble J.(1994). GLP-1 is localized to the mitotic region of the C. elegans germ line. Development (Cambridge, England) 120, 2901–2911.

de la Cova C, and Greenwald I.(2012). SEL-10/Fbw7-dependent negative feedback regulation of LIN-45/Braf signaling in C. elegans via a conserved phosphodegron. Genes & development 26, 2524–2535. [PubMed: 23154983]

de la Cova C, Townley R, Regot S, and Greenwald I.(2017). A Real-Time Biosensor for ERK Activity Reveals Signaling Dynamics during C elegans Cell Fate Specification. Developmental Cell 42, 542–553.e544. [PubMed: 28826819]

Deng Y, and Greenwald I.(2016). Determinants in the LIN-12/Notch Intracellular Domain That Govern Its Activity and Stability During Caenorhabditis elegans Vulval Development. G3 Genes|Genomes|Genetics 6, 3663–3670. [PubMed: 27646703]

Diaz-Cuadros M, Pourquié O, and El-Sherif E.(2021). Patterning with clocks and genetic cascades: Segmentation and regionalization of vertebrate versus insect body plans. PLOS Genetics 17, e1009812.

Dickinson DJ, Pani AM, Heppert JK, Higgins CD, and Goldstein B.(2015). Streamlined Genome Engineering with a Self-Excising Drug Selection Cassette. Genetics 200, 1035–1049. [PubMed: 26044593]

Edwards SL, Charlie NK, Milfort MC, Brown BS, Gravlin CN, Knecht JE, and Miller KG (2008). A Novel Molecular Solution for Ultraviolet Light Detection in Caenorhabditis elegans. PLOS Biology 6, e198. [PubMed: 18687026]

El Mouridi S, Lecroisey C, Tardy P, Mercier M, Leclercq-Blondel A, Zariohi N, and Boulin T.(2017). Reliable CRISPR/Cas9 Genome Engineering in Caenorhabditis elegans Using a Single Efficient sgRNA and an Easily Recognizable Phenotype. G3 Genes|Genomes|Genetics 7, 1429–1437. [PubMed: 28280211]

Falo-Sanjuan J, and Bray SJ (2020). Decoding the Notch signal. Development, Growth & Differentiation 62, 4–14.

Falo-Sanjuan J., Lammers NC., Garcia HG., and Bray SJ. (2019). Enhancer Priming Enables Fast and Sustained Transcriptional Responses to Notch Signaling. Developmental Cell 50, 411–425.e418. [PubMed: 31378591]

Foehr ML, and Liu J.(2008). Dorsoventral patterning of the C. elegans postembryonic mesoderm requires both LIN-12/Notch and TGFbeta signaling. Developmental biology 313, 256–266. [PubMed: 18036582]

Frøkjær-Jensen C, Davis MW, Ailion M, and Jorgensen EM (2012). Improved Mos1-mediated transgenesis in C. elegans. Nature Methods 9, 117–118. [PubMed: 22290181]

Frøkjær-Jensen C, Davis MW, Sarov M, Taylor J, Flibotte S, LaBella M, Pozniakovsky A, Moerman DG, and Jorgensen EM (2014). Random and targeted transgene insertion in Caenorhabditis elegans using a modified Mos1 transposon. Nature Methods 11, 529–534. [PubMed: 24820376]

Gauthier K, and Rocheleau CE (2017). C. elegans Vulva Induction: An In Vivo Model to Study Epidermal Growth Factor Receptor Signaling and Trafficking. In ErbB Receptor Signaling Methods in Molecular Biology, Wang Z, ed. (New York, NY: Humana Press).

Gibson DG, Young L, Chuang R-Y, Venter JC, Hutchison CA, and Smith HO (2009). Enzymatic assembly of DNA molecules up to several hundred kilobases. Nature Methods 6, 343–345. [PubMed: 19363495]

Greenwald I.(2012). *Notch* and the Awesome Power of Genetics. Genetics 191, 655. [PubMed: 22785620]

Greenwald I, and Kovall R.(2013). Notch signaling: genetics and structure. WormBook : the online review of C elegans biology, 1–28.

Greenwald I, Sternberg PW, and Horvitz HR (1983). The lin-12 locus specifies cell fates in Caenorhabditis elegans. Cell, 435–444.

Gutnik S, Thomas Y, Guo Y, Stoecklin J, Neagu A, Pintard L, Merlet J, and Ciosk R.(2018). PRP-19, a conserved pre-mRNA processing factor and E3 ubiquitin ligase, inhibits the nuclear accumulation of GLP-1/Notch intracellular domain. Biology Open 7, bio034066.

Hale JJ, Amin NM, George C, Via Z, Shi H, and Liu J.(2014). A role of the LIN-12/Notch signaling pathway in diversifying the non-striated egg-laying muscles in C. elegans. Developmental biology 389, 137–148. [PubMed: 24512688]

Hansson EM, Teixeira AI, Gustafsson MV, Dohda T, Chapman G, Meletis K, Muhr J, and Lendahl U.(2006). Recording Notch Signaling in Real Time. Developmental Neuroscience 28, 118–127. [PubMed: 16508309]

Harfe BD, Gomes AV, Kenyon C, Liu J, Krause M, and Fire A.(1998). Analysis of a Caenorhabditis elegans Twist homolog identifies conserved and divergent aspects of mesodermal patterning. Genes & development 12, 2623–2635. [PubMed: 9716413]

Heitzler P, Bourouis M, Ruel L, Carteret C, and Simpson P.(1996). Genes of the Enhancer of split and achaete-scute complexes are required for a regulatory loop between Notch and Delta during lateral signalling in Drosophila. Development (Cambridge, England) 122, 161–171.

Henrique D, and Schweisguth F.(2019). Mechanisms of Notch signaling: a simple logic deployed in time and space. Development (Cambridge, England) 146.

Ho C, and Morsut L.(2021). Novel synthetic biology approaches for developmental systems. Stem Cell Reports 16, 1051–1064. [PubMed: 33979593]

Housden BE, Li J, Bray SJ, Marathe S, Alberi L, Ilagan MXG, Kopan R, Shimojo H, Harima Y, and Kageyama R.(2014). In Notch signaling Methods in Molecular Biology (Methods and Protocols), Bellen HJ, and Yamamoto S, eds. (New York, NY: Humana Press), pp. 101–180.

Hubaud A, and Pourquié O.(2014). Signalling dynamics in vertebrate segmentation. Nature Reviews Molecular Cell Biology 15, 709–721. [PubMed: 25335437]

Hubaud A, Regev I, Mahadevan L, and Pourquié O.(2017). Excitable Dynamics and Yap-Dependent Mechanical Cues Drive the Segmentation Clock. Cell 171, 668–682.e611. [PubMed: 28942924]

Hubbard EJA, and Schedl T.(2019). Biology of the Caenorhabditis elegans Germline Stem Cell System. Genetics 213, 1145–1188. [PubMed: 31796552]

Hubbard EJA, Wu G, Kitajewski J, and Greenwald I.(1997). sel-10, a negative regulator of lin-12 activity inCaenorhabditis elegans, encodes a member of the CDC4 family of proteins. Genes & development 11, 3182–3193. [PubMed: 9389650]

Hung YP, Teragawa C, Kosaisawe N, Gillies TE, Pargett M, Minguet M, Distor K, Rocha-Gregg BL, Coloff JL, Keibler MA, et al. (2017). Akt regulation of glycolysis mediates bioenergetic stability in epithelial cells. eLife 6, e27293. [PubMed: 29239720]

Hunter GL, and Giniger E.(2020). Phosphorylation and Proteolytic Cleavage of Notch in Canonical and Noncanonical Notch Signaling. In Notch signaling in Embryology and Cancer Advances in Experimental Medicine and Biology, Reichrath J, and Reichrath S, eds. (Cham: Springer).

Hyrenius-Wittsten A, Su Y, Park M, Garcia Julie M, Alavi J, Perry N, Montgomery G, Liu B, and Roybal Kole T.(2021). SynNotch CAR circuits enhance solid tumor recognition and promote persistent antitumor activity in mouse models. Science Translational Medicine 13, eabd8836.

Ilagan MXG, Lim S, Fulbright M, Piwnica-Worms D, and Kopan R.(2011). Real-Time Imaging of Notch Activation with a Luciferase Complementation-Based Reporter. Science Signaling 4, rs7-rs7.

Inagaki HK., Ben-Tabou de-Leon S., Wong AM., Jagadish S., Ishimoto H., Barnea G., Kitamoto T., Axel R., and Anderson DJ. (2012). Visualizing neuromodulation in vivo: TANGO-mapping of dopamine signaling reveals appetite control of sugar sensing. Cell 148, 583–595. [PubMed: 22304923]

Johnson HE, and Toettcher JE (2019). Signaling Dynamics Control Cell Fate in the Early Drosophila Embryo. Developmental Cell 48, 361–370.e363. [PubMed: 30753836]

Kamentsky L, Jones TR, Fraser A, Bray M-A, Logan DJ, Madden KL, Ljosa V, Rueden C, Eliceiri KW, and Carpenter AE (2011). Improved structure, function and compatibility for CellProfiler: modular high-throughput image analysis software. Bioinformatics 27, 1179–1180. [PubMed: 21349861]

Kannan R, Cox E, Wang L, Kuzina I, Gu Q, and Giniger E.(2018). Tyrosine phosphorylation and proteolytic cleavage of Notch are required for non-canonical Notch/Abl signaling in Drosophila axon guidance. Development (Cambridge, England) 145, dev151548.

Kapust RB, Tözsér J, Copeland TD, and Waugh DS (2002). The P1′ specificity of tobacco etch virus protease. Biochemical and Biophysical Research Communications 294, 949–955. [PubMed: 12074568]

Karp X, and Greenwald I. (2003). Post-transcriptional regulation of the E/Daughterless ortholog HLH-2, negative feedback, and birth order bias during the AC/VU decision in C. elegans. Genes Dev 17, 3100–3111. 10.1101/gad.1160803. [PubMed: 14701877]

Karp X, and Greenwald I. (2004). Multiple roles for the E/Daughterless ortholog HLH-2 during C. elegans gonadogenesis. Dev Biol 272, 460–469. 10.1016/j.ydbio.2004.05.015. [PubMed: 15282161]

Katow H, Takahashi T, Saito K, Tanimoto H, and Kondo S.(2019). Tango knock-ins visualize endogenous activity of G protein-coupled receptors in Drosophila. Journal of Neurogenetics 33, 44–51. [PubMed: 31084242]

Keil W, Kutscher LM, Shaham S, and Siggia ED (2017). Long-term highresolution imaging of developing C. elegans larvae with microfluidics. Dev Cell 40, 202–214. 10.1016/j.devcel.2016.11.022. [PubMed: 28041904]

Kershner AM, Shin H, Hansen TJ, and Kimble J.(2014). Discovery of two GLP-1/Notch target genes that account for the role of GLP-1/Notch signaling in stem cell maintenance. Proceedings of the National Academy of Sciences 111, 3739–3744.

Kim H, Ishidate T, Ghanta KS, Seth M, Conte D, Shirayama M, and Mello CC (2014). A Co-CRISPR Strategy for Efficient Genome Editing in *Caenorhabditis elegans*. Genetics 197, 1069–1080. [PubMed: 24879462]

Krebs LT, Xue Y, Norton CR, Shutter JR, Maguire M, Sundberg JP, Gallahan D, Closson V, Kitajewski J, Callahan R, et al. (2000). Notch signaling is essential for vascular morphogenesis in mice. Genes & development 14, 1343–1352. [PubMed: 10837027]

Kroetz MB, and Zarkower D.(2015). Cell-Specific mRNA Profiling of the Caenorhabditis elegans Somatic Gonadal Precursor Cells Identifies Suites of Sex-Biased and Gonad-Enriched Transcripts. G3: Genes|Genomes|Genetics 5, 2831–2841. [PubMed: 26497144]

Lambie EJ, and Kimble J.(1991). Two homologous regulatory genes, lin-12 and glp-1, have overlapping functions. Development (Cambridge, England) 112, 231–240.

Lecourtois M, and Schweisguth F.(1998). Indirect evidence for Delta-dependent intracellular processing of Notch in Drosophila embryos. Current Biology 8, 771–775. [PubMed: 9651681]

Lee C, Shin H, and Kimble J.(2019). Dynamics of Notch-Dependent Transcriptional Bursting in Its Native Context. Developmental Cell 50, 426–435.e424. [PubMed: 31378588]

Lee C, Sorensen EB, Lynch TR, and Kimble J.(2016). C. elegans GLP-1/Notch activates transcription in a probability gradient across the germline stem cell pool. eLife 5, e18370. [PubMed: 27705743]

Levitan D, and Greenwald I.(1998). LIN-12 protein expression and localization during vulval development in C. elegans. Development (Cambridge, England) 125, 3101–3109.

Li J.(2011). Temporal control of Vulval Precursor Cell fate patterning in Caenorhabditis elegans (Columbia University).

Li P., Collins KM., Koelle MR., and Shen K. (2013). LIN-12/Notch signaling instructs postsynaptic muscle arm development by regulating UNC-40/DCC and MADD-2 in Caenorhabditis elegans. eLife 2, e00378. [PubMed: 23539368]

Liu Z, Brunskill E, Boyle S, Chen S, Turkoz M, Guo Y, Grant R, and Kopan R.(2015). Second-generation Notch1 activity-trap mouse line (N1IP::CreHI) provides a more comprehensive map of cells experiencing Notch1 activity. Development (Cambridge, England) 142, 1193–1202.

Luo KL, Underwood RS, and Greenwald I.(2020). Positive autoregulation of *lag-1* in response to LIN-12 activation in cell fate decisions during *C. elegans* reproductive system development. Development (Cambridge, England) 147, dev193482.

Merritt C, Rasoloson D, Ko D, and Seydoux G.(2008). 3′ UTRs Are the Primary Regulators of Gene Expression in the C. elegans Germline. Current Biology 18, 1476–1482. [PubMed: 18818082]

Morsut L, Roybal Kole T., Xiong X, Gordley Russell M., Coyle Scott M., Thomson M, and Lim Wendell A. (2016). Engineering Customized Cell Sensing and Response Behaviors Using Synthetic Notch Receptors. Cell 164, 780–791. [PubMed: 26830878]

Nandagopal N, Santat LA, LeBon L, Sprinzak D, Bronner ME, and Elowitz MB (2018). Dynamic Ligand Discrimination in the Notch Signaling Pathway. Cell 172, 869–880.e819. [PubMed: 29398116]

Newman AP, White JG, and Sternberg PW (1995). The Caenorhabditis elegans lin-12 gene mediates induction of ventral uterine specialization by the anchor cell. Development (Cambridge, England) 121, 263–271.

Pani AM, and Goldstein B.(2018). Direct visualization of a native Wnt in vivo reveals that a long-range Wnt gradient forms by extracellular dispersal. eLife 7, e38325. [PubMed: 30106379]

Pokrass MJ, Ryan KA, Xin T, Pielstick B, Timp W, Greco V, and Regot S.(2020). Cell-Cycle-Dependent ERK Signaling Dynamics Direct Fate Specification in the Mammalian Preimplantation Embryo. Developmental Cell 55, 328–340.e325. [PubMed: 33091369]

Pompa de la JL, Wakeham A, Correia KM, Samper E, Brown S, Aguilera RJ, Nakano T, Honjo T, Mak TW, Rossant J, et al. (1997). Conservation of the Notch signalling pathway in mammalian neurogenesis. Development (Cambridge, England) 124, 1139–1148.

Priess JR, Schnabel H, and Schnabel R.(1987). The glp-1 locus and cellular interactions in early C. elegans embryos. Cell 51, 601–611. [PubMed: 3677169]

Purvis Jeremy E., and Lahav G.(2013). Encoding and Decoding Cellular Information through Signaling Dynamics. Cell 152, 945–956. [PubMed: 23452846]

Regot S, Hughey Jacob J., Bajar Bryce T., Carrasco S, and Covert Markus W. (2014). High-Sensitivity Measurements of Multiple Kinase Activities in Live Single Cells. Cell 157, 1724–1734. [PubMed: 24949979]

Roybal KT, Williams JZ, Morsut L, Rupp LJ, Kolinko I, Choe JH, Walker WJ, McNally KA, and Lim WA (2016). Engineering T Cells with Customized Therapeutic Response Programs Using Synthetic Notch Receptors. Cell 167, 419–432.e416. [PubMed: 27693353]

Ruijtenberg S, and van den Heuvel S.(2015). G1/S Inhibitors and the SWI/SNF Complex Control Cell-Cycle Exit during Muscle Differentiation. Cell 162, 300–313. [PubMed: 26144318]

Ryu H, Chung M, Dobrzyński M, Fey D, Blum Y, Lee SS, Peter M, Kholodenko BN, Jeon NL, and Pertz O.(2015). Frequency modulation of ERK activation dynamics rewires cell fate. Molecular systems biology 11, 838. [PubMed: 26613961]

Sallee MD, Aydin T, and Greenwald I.(2015). Influences of LIN-12/Notch and POP-1/TCF on the Robustness of Ventral Uterine Cell Fate Specification in Caenorhabditis elegans Gonadogenesis. G3 Genes|Genomes|Genetics 5, 2775–2782. [PubMed: 26483009]

Sallee MD, Aydin T, and Greenwald I. (2015). Influences of LIN-12/Notch and POP-1/TCF on the robustness of ventral uterine cell fate specification in Caenorhabditis elegans gonadogenesis. G3 5, 2775–2782. 10.1534/g3.115.022608. [PubMed: 26483009]

Sfarcic I, Bui T, Daniels EC, and Troemel ER (2019). Nanoluciferase-Based Method for Detecting Gene Expression in Caenorhabditis elegans. Genetics 213, 1197–1207. [PubMed: 31585955]

Shaffer JM, and Greenwald I.(2022). Floxed exon (Flexon): A flexibly positioned stop cassette for recombinase-mediated conditional gene expression. Proceedings of the National Academy of Sciences 119, e2117451119.

Shaye DD, and Greenwald I.(2002). Endocytosis-mediated downregulation of LIN-12/Notch upon Ras activation in Caenorhabditis elegans. Nature 420, 686–690. [PubMed: 12478297]

Shin H, and Reiner DJ (2018). The Signaling Network Controlling C. elegans Vulval Cell Fate Patterning. Journal of Developmental Biology 6, 30.

Simon CS, Rahman S, Raina D, Schröter C, and Hadjantonakis A-K (2020). Live Visualization of ERK Activity in the Mouse Blastocyst Reveals Lineage-Specific Signaling Dynamics. Developmental Cell 55, 341–353.e345. [PubMed: 33091370]

Sorensen EB, Seidel HS, Crittenden SL, Ballard JH, and Kimble J. (2020). A toolkit of tagged glp-1 alleles reveals strong glp-1 expression in the germline, embryo, and spermatheca. MicroPubl. Biol https://www.micropublication.org/journals/biology/micropub-biology-000271.

Souilhol C, Cormier S, Monet M, Vandormael-Pournin S, Joutel A, Babinet C, and Cohen-Tannoudji M.(2006). Nas transgenic mouse line allows visualization of Notch pathway activity in vivo. genesis 44, 277–286. [PubMed: 16708386]

Srivastava S, Salter AI, Liggitt D, Yechan-Gunja S, Sarvothama M, Cooper K, Smythe KS, Dudakov JA, Pierce RH, Rader C, et al. (2019). Logic-Gated ROR1 Chimeric Antigen Receptor Expression Rescues T Cell-Mediated Toxicity to Normal Tissues and Enables Selective Tumor Targeting. Cancer Cell 35, 489–503.e488. [PubMed: 30889382]

Sternberg PW (2005). Vulval development. In WormBook : the online review of C elegans biology, T.C.e.R. Community, ed., pp. 1–28.

Stiernagle T.(2006). Maintenance of C. elegans. WormBook : the online review of C elegans biology, 1–11.

Struhl G, and Adachi A.(1998). Nuclear Access and Action of Notch In Vivo. Cell 93, 649–660. [PubMed: 9604939]

Sulston JE, and Horvitz HR (1977). Post-embryonic cell lineages of the nematode, Caenorhabditis elegans. Developmental biology 56, 110–156. [PubMed: 838129]

Sundaram MV (2005). The love–hate relationship between Ras and Notch. Genes & development 19, 1825–1839. [PubMed: 16103211]

Tan PB, Lackner MR, and Kim SK (1998). MAP kinase signaling specificity mediated by the LIN-1 Ets/LIN-31 WH transcription factor complex during C. elegans vulval induction. Cell 93, 569–580. [PubMed: 9604932]

Tenen CC, and Greenwald I.(2019). Cell Non-autonomous Function of daf-18/PTEN in the Somatic Gonad Coordinates Somatic Gonad and Germline Development in C. elegans Dauer Larvae. Current biology : CB 29, 1064–1072.e1068. [PubMed: 30827916]

Viswanathan R, Necakov A, Trylinski M, Harish RK, Krueger D, Esposito E, Schweisguth F, Neveu P, and De Renzis S.(2019). Optogenetic inhibition of Delta reveals digital Notch signalling output during tissue differentiation. EMBO reports 20, e47999. [PubMed: 31668010]

Vooijs M, Ong C-T, Hadland B, Huppert S, Liu Z, Korving J, van den Born M, Stappenbeck T, Wu Y, Clevers H, et al. (2007). Mapping the consequence of Notch1 proteolysis in vivo with NIP-CRE. Development (Cambridge, England) 134, 535–544.

Ward A, Liu J, Feng Z, and Xu XZS (2008). Light-sensitive neurons and channels mediate phototaxis in C. elegans. Nature Neuroscience 11, 916–922. [PubMed: 18604203]

Ward JD (2015). Rapid and Precise Engineering of the Caenorhabditis elegans Genome with Lethal Mutation Co-Conversion and Inactivation of NHEJ Repair. Genetics 199, 363–377. [PubMed: 25491644]

Welcker M, and Clurman BE (2008). FBW7 ubiquitin ligase a tumour suppressor at the crossroads of cell division, growth and differentiation. Nature Reviews Cancer 8, 83–93. [PubMed: 18094723]

Wilkinson HA., Fitzgerald K., and Greenwald I. (1994). Reciprocal changes in expression of the receptor lin-12 and its ligand lag-2 prior to commitment in a C. elegans cell fate decision. Cell 79, 1187–1198. [PubMed: 8001154]

Xu D, Farmer A, Collett G, Grishin NV, and Chook YM (2012). Sequence and structural analyses of nuclear export signals in the NESdb database. Molecular biology of the cell 23, 3677–3693. [PubMed: 22833565]

Yoo AS, Bais C, and Greenwald I.(2004). Crosstalk between the EGFR and LIN-12/Notch pathways in C. elegans vulval development. Science (New York, NY) 303, 663–666.

Yoo AS, and Greenwald I.(2005). LIN-12/Notch Activation Leads to MicroRNA-Mediated Down-Regulation of Vav in *C. elegans*. Science (New York, NY) 310, 1330–1333.

Zacharioudaki E, and Bray SJ (2014). Tools and methods for studying Notch signaling in Drosophila melanogaster. Methods 68, 173–182. [PubMed: 24704358]

Highlights

- SALSA is a genetically encoded Notch biosensor based on GFP localization
- SALSA has been validated for the *C. elegans* Notch homologs LIN-12 and GLP-1
- Time-lapse imaging using SALSA illuminates a stochastic LIN-12-mediated decision
- SALSA should be general to other systems and adaptable for SynNotch applications

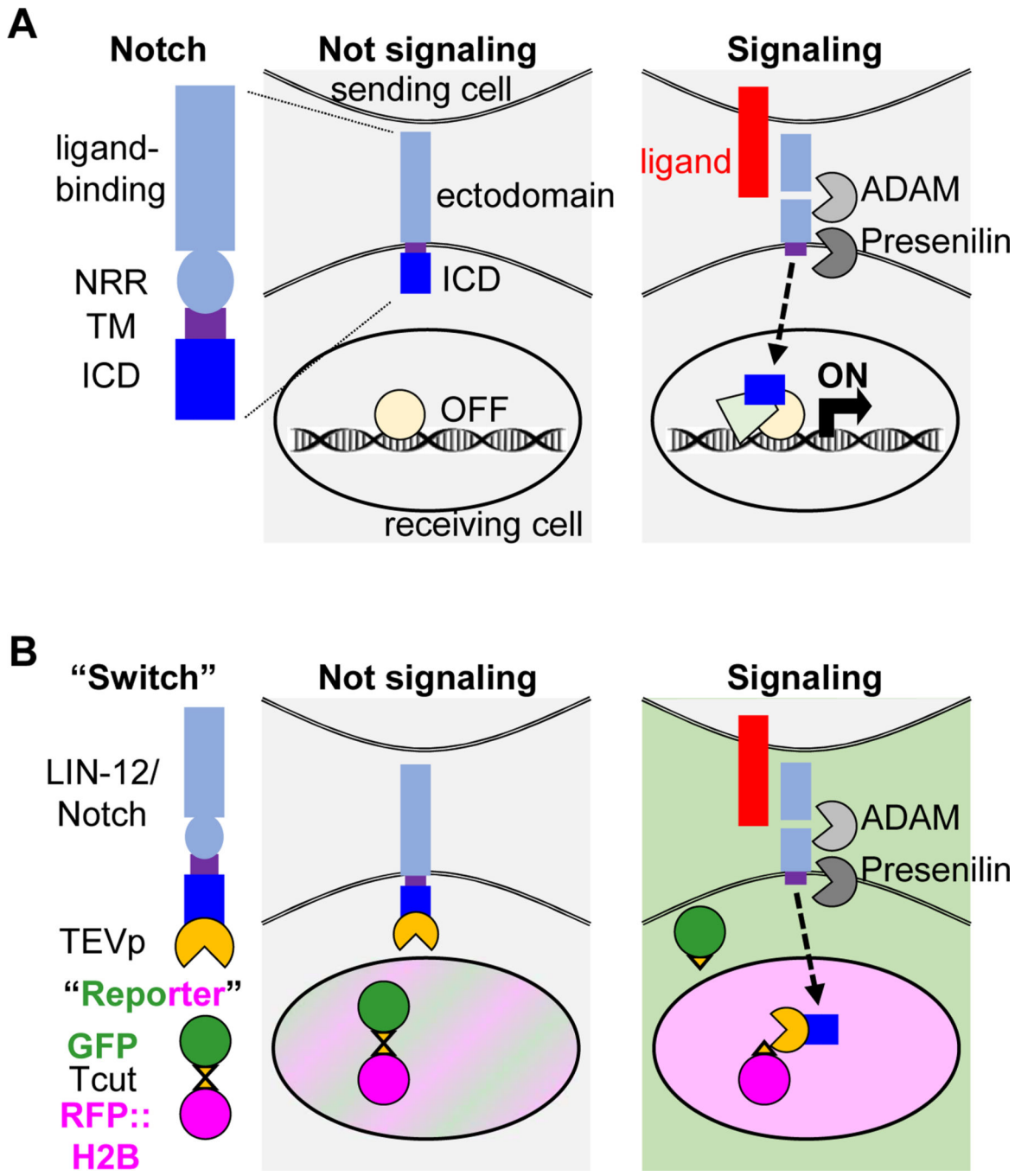

Figure 1. SALSA design

(A) The intracellular domain of Notch is a membrane tethered transcriptional activator. When Notch is inactive, the intracellular domain (ICD) remains at the cell membrane and target gene transcription is repressed by a sequence-specific DNA binding protein of the CSL family, which in the absence of Notch activation is associated with co-repressors. When Notch interacts with ligand, cleavage in the ectodomain by an ADAM protease followed by cleavage in the transmembrane domain by Presenilin, the catalytic component of the γ-secretase complex, releases the ICD from the membrane. ICD enters the

nucleus and forms the Notch nuclear complex with CSL and other coactivators to promote transcription of target genes (reviewed in Falo-Sanjuan and Bray, 2020; Greenwald and Kovall, 2013; Henrique and Schweisguth, 2019).

(B) SALSA is a bipartite Notch activity sensor, consisting of a "switch" and cleavable "reporter." The "switch" is Notch fused to TEV protease (TEVp). The cleavable "reporter" is a fusion protein that contains GFP tethered to the nucleus by an RFP::H2B, with an intervening TEV protease recognition site (Tcut). When Notch is inactive, TEVp does not gain access to the nucleus, so the reporter is uncleaved and the nuclear Red:Green ratio is low; when Notch is activated, TEVp-tagged ICD enters the nucleus and cleaves the reporter, releasing GFP from the RFP::H2B tether to diffuse out of the nucleus, resulting in a high nuclear Red:Green ratio.

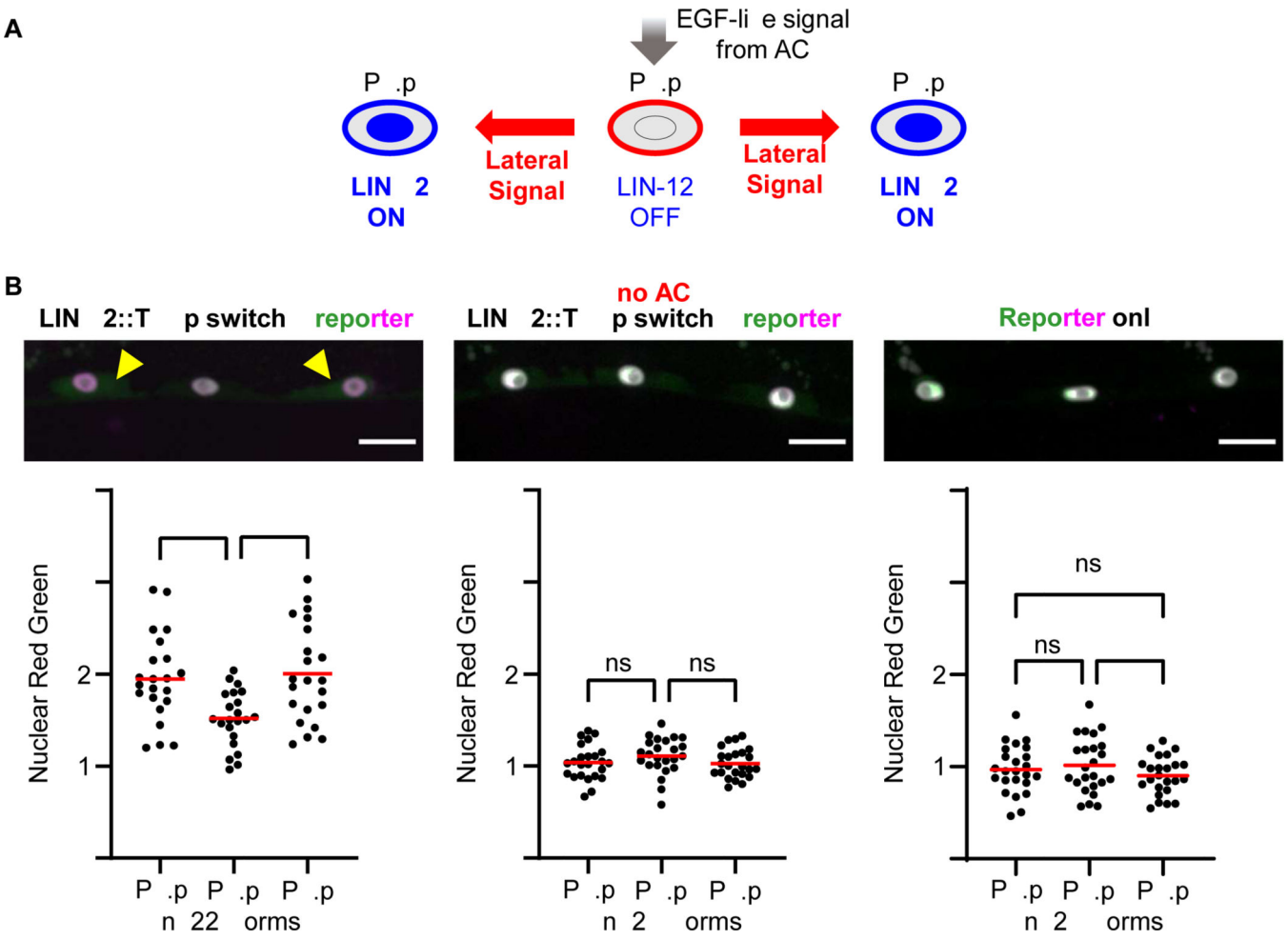

Figure 2. SALSA agrees with expectations for LIN-12/Notch activity in in the Vulval Precursor Cells (VPCs).

(A) Schematic representation of LIN-12/Notch activity in VPCs and descendants. Three VPCs, named P5.p, P6.p, and P7.p, are patterned during the L3 stage by a combination of LET-23/EGF Receptor and LIN-12/Notch activity (Gauthier and Rocheleau, 2017; Shin and Reiner, 2018; Sternberg, 2005). An EGF-like inductive signal from the Anchor Cell (AC) of the gonad induces P6.p to express the lateral signal, consisting of ligands for LIN-12. These ligands activate LIN-12 in P5.p and P7.p. There are multiple regulatory mechanisms that ensure that LIN-12 is maximally activated in P5.p and P7.p, and LET-23/EGFR is maximally activated in P6.p (Sundaram, 2005). These mechanisms include multiple direct transcriptional targets of LIN-12 that antagonize EGFR activity in P5.p and P7.p (Berset et al., 2001; Yoo et al., 2004), and of LET-23/EGFR that lead to loss of LIN-12 protein in P6.p (Levitan and Greenwald, 1998; Shaye and Greenwald, 2002).

(B) SALSA agrees with expectations based on genetic analysis and LIN-12/Notch transcriptional target reporters in VPCs. Photomicrographs are maximum orthogonal projections for all Z planes with visible fluorescence. Scale bars are 10 μm. Yellow arrowhead, cytoplasmic GFP.

For each genotype, we performed an RM one-way ANOVA to compare the nuclear Red:Green ratios in the VPCs. There was a statistically significant difference in nuclear

Red:Green ratios between the VPCs in the presence of the LIN-12::TEVp switch (left, $F(2,21)=18.24$, $p<0.0001$). Post hoc comparisons (STAR Methods) indicate that there is a significantly higher nuclear Red:Green fluorescence in P5.p and P7.p compared to P6.p (****$p<0.0001$). Center, when the AC is eliminated, LIN-12/Notch is not activated in P5.p and P7.p, and there was no statistically significant difference in nuclear Red:Green ratio between the VPCs ($F(2,23)=2.143$, $p=0.1337$). In the reporter only genotype, a low statistically significant difference was seen ($F(2,23)=4.661$, $p<0.05$); post hoc comparisons (STAR Methods) indicated a slight difference between P6.p and P7.p in the reporter only control (*$p<0.05$), but not between P5.p and either other VPC ($p>0.05$), suggesting that the slight difference is not biologically meaningful. See also Figure S1 for analysis of a *sel-10/FBXW7* E3 ubiquitin ligase mutant.

We also performed ordinary one-way ANOVAs to compare P5.p and P7.p between genotypes, and found significant differences (P5.p, $F(2,67)=63.37$, $p<0.0001$; P7.p, $F(2,67)=72.84$, $p<0.0001$). Post hoc comparisons (STAR methods) revealed that in the presence of the LIN-12:TEVp switch and an AC, P5.p and P7.p had significantly higher nuclear Red:Green ratios than in the absence of the switch or the absence of the AC (****$p<0.0001$), but there was no difference in nuclear Red:Green ratios between the no AC and the reporter only genotypes for both P5.p and P7.p ($p>0.05$).

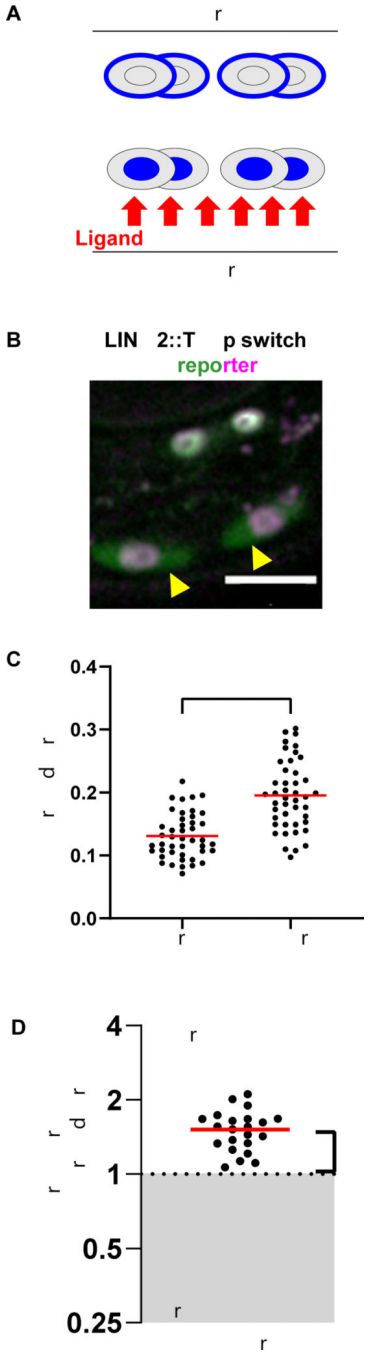

Figure 3. SALSA agrees with expectations for LIN-12/Notch activity in the M lineage of *C. elegans.*

(A) Schematic representation of LIN-12/Notch activity in the M lineage. Both dorsal and ventral descendants of the M mesoblast express LIN-12, but LIN-12 is activated only in the ventral descendants by ligand from the ventral hypodermis (Foehr and Liu, 2008).

(B) Visual evidence that LIN-12 is active in ventral but not dorsal M descendants. Photomicrograph is one Z slice taken at the 8-M stage of a hermaphrodite carrying the LIN-12::TEVp switch and the cleavable reporter expressed in the M lineage (strain

GS9399). At this stage, four of the eight cells are on the right, and the other four are on the left; this slice captures one side. Yellow arrowhead, cytoplasmic GFP is readily apparent. Scale bar is 10 μm. See Figure S3 for time-lapse videos of three worms.

(C) Nuclear Red:Green quantification at the 8-M stage. Red lines indicate the mean. The nuclear Red:Green ratio was significantly higher in ventral cells than in dorsal cells (Unpaired ttest, t(168)=8.699, ****p<0.0001). See Figure S2 for alternative quantification strategies.

(D) On a per-animal basis, the nuclear Red:Green ratio is greater in ventral cells compared to dorsal cells. Each point represents the ratio of the average nuclear Red:Green between the ventral cells and dorsal cells within each animal from (C). When compared to a null hypothesis of the dorsal and ventral cells having equivalent LIN-12 activity (a ratio of 1), the mean was significantly greater than 1, indicating that the average nuclear Red:Green ratio is greater in ventral cells than dorsal cells (One sample t-test, t(21)=27.95, ****p<0.0001).

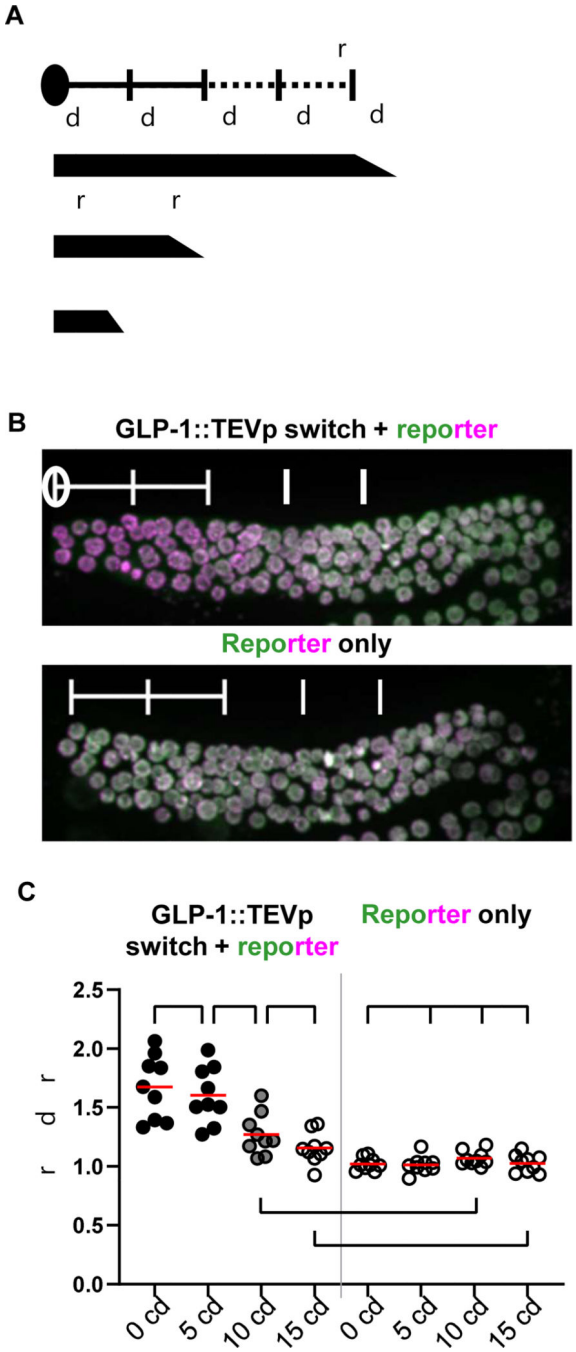

Figure 4. SALSA agrees with expectations for GLP-1 Notch activity in the germ line of *C. elegans*.

(A) Schematic representation of GLP-1 activity and expression of transcriptional targets in the germ line. GLP-1 activity peaks in Germline Stem Cells (GSCs) within 5 cell diameters (cd) of the distal end of the gonad arm; GLP-1 activity is detectable throughout the GSC pool ~8–10 cd from the distal end (see text).

(B) SALSA detects GLP-1 activity in GSCs at the distal end of the gonad arm. Each photomicrograph shows a single gonad arm from an L4 larva. See STAR Methods for

measurement details. The reddened distal end of the germ line from the larvae expressing the GLP-1::TEVp switch correlates with the known pattern of GLP-1 activity.

(C) GLP-1 activity peaks from 0–5 cd, ceases by ~10 cd. Each dot represents one germ nucleus; red lines indicate the mean. A one-way ANOVA found a significant effect of the position of the cells in the presence of the switch on nuclear Red:Green ratio in GSCs ($F(7, 64) = 26.16$, $p<0.0001$). Post hoc pairwise comparisons showed that in the presence of the GLP-1::TEVp switch, nuclear Red:Green significantly decreased between 5 and 10 cd (***$p<0.001$). The nuclear Red:Green ratio for 10 cd was not significantly different from 15 cd, and neither were significantly different from the same relative position in the reporter only control ($p>0.05$). In the absence of the GLP-1::TEVp switch, all regions had similar nuclear Red:Green ratios ($p>0.05$).

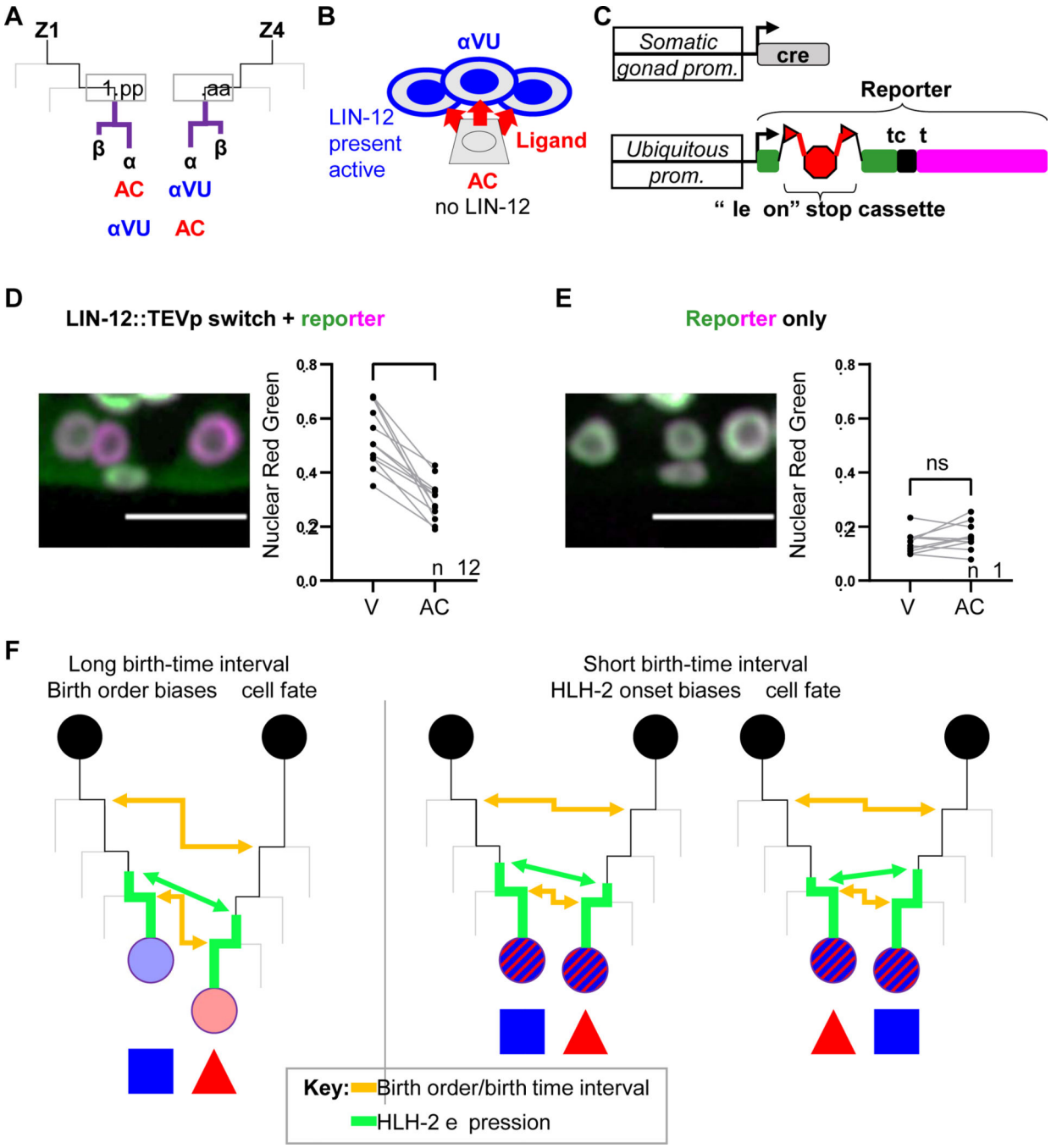

Figure 5. SALSA agrees with expectations for LIN-12 activity in the committed AC and VU.

(A) Lineal origin of the α cells. The somatic gonad precursor cells Z1 and Z4 give rise to the α cells, Z1.ppp and Z4.aaa, which undergo a, binary cell fate decision to ensure one becomes the AC and the other the αVU. The sisters of the α cells, called the β cells, always become VUs; they do not strictly require *lin-12* activity for VU fate (Sallee et al., 2015) and are not considered further here. The parents of the α cells are Z1.pp and Z4.aa.

(B) Schematic representation of LIN-12 activity in the proximal somatic gonad in the early L3 stage. LAG-2 and LIN-12 are initially expressed in both α cells, but during the

AC/VU decision, feedback loops lead to reciprocal expression patterns that are sustained in the committed progeny. The differentiated AC expresses the ligand LAG-2, and the αVU expresses LIN-12 as well as reporters for transcriptional targets of LIN-12 (Luo et al., 2020; Yoo and Greenwald, 2005).

(C) Diagram of the "somatic gonad cleavable reporter" transgenes. One transgene (*arTi237*) drives expression of Cre recombinase in Z1 and Z4, leading to excision of a *flexon* stop cassette from transgene *arTi355*, allowing for strong, specific expression of GFP::Tcut::mScarlet::H2B from a pan-somatic ribosomal protein gene promoter (STAR Methods; Shaffer and Greenwald, 2022).

(D) SALSA agrees with expectations that LIN-12 is active in the αVU and not in the AC. The photomicrograph is a maximum orthogonal projection of an individual expressing the LIN-12::TEVp switch and the somatic gonad cleavable reporter in early L3. Scale bar is 10 μm. The early L3 hermaphrodite displays visibly reddened VU nuclei. The nuclear Red:Green ratio for the αVU is statistically higher than the AC (paired t-test, t=7.932, df=11, ****p<0.0001). Regardless of the absolute value, the nuclear Red:Green ratio in the αVU is always higher than the AC in any given animal in the presence of the LIN-12::TEVp switch.

(E) Reporter only control for D. The photomicrograph is a maximum orthogonal projection of all Z planes with visible fluorescence of an individual expressing only the reporter. Scale bar is 10 μm. No significant difference between the AC and αVU was seen was seen in nuclear Red:Green quantitation (paired t-test, t=1.514, df=9, p=0.1644).

(F) Two stochastic elements prior to the birth of the α cells bias the outcome of the AC/VU decision. The birth-time interval is indicated by yellow double-headed arrows, and HLH-2 expression is indicated in green. See text for details.

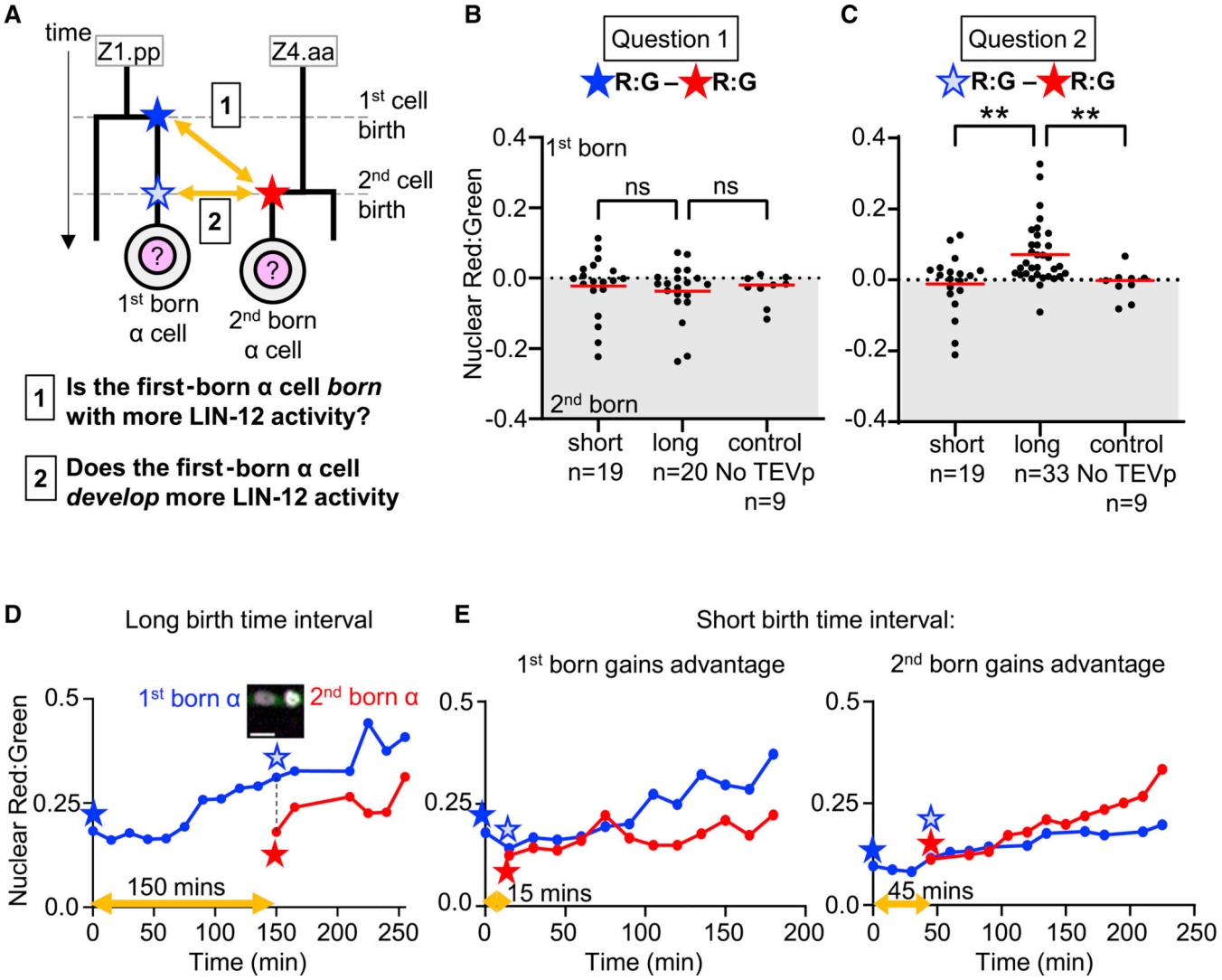

Figure 6. SALSA provides evidence for the proposed activity of LIN-12 with respect to stochastic events that influence the AC/VU decision.

(A) Schematic diagram of critical timepoints. The solid blue star represents the first-born α cell immediately after its birth, and the blue outlined star represents the first-born α cell at the time that the second-born cell is born (solid red star). The yellow double-arrowed lines indicate the comparisons made in (B) and (C) to answer the questions posed below the diagram. See Figure S4 for ten time-lapse videos of SALSA across the timepoints represented here.

(B) Each α cell is born with a similar level of LIN-12 activity, regardless of birth-time interval or relative birth-order. We determined the difference in nuclear Red:Green ratio between the first-born and second-born α cells at the timepoint after each of their birth. Each α cell pair was binned into short and long birth-time intervals for animals expressing the LIN-12::TEVp switch and somatic gonad cleavable reporter (STAR Methods) and the bins were compared to each other and to a cleavable reporter only control. Each dot represents one cell α pair, and the red lines indicate the mean. No significant difference was seen after statistical analysis (Kruskal-Wallis, H = 1.196, df = 3, p = 0.55). See Figure S5 for

quantitation of SALSA in the parents of the α cells, and STAR methods for details of quantitation and statistical tests. For both strains, only animals in which both α cell births were captured and able to be quantified were included in this analysis.

(C) When the birth-time interval is long, the first-born α cell gains a relative advantage in LIN-12 activity. We determined the difference in nuclear Red:Green ratio between the first-born and second-born α cells at the timepoint after the birth of the second-born cell. Animals were binned and the difference in nuclear Red:Green ratio compared as in (B). Kruskal-Wallis tests indicated significant differences between the groups ($H = 16.26$, $df = 3$, $p=0.0003$). Post hoc pairwise comparisons (STAR Methods) find the long birth-time interval bin had significantly greater differences in nuclear Red:Green ratio between α cells than in the short birth-time interval bin or cleavable reporter only control (**$p<0.01$). Animals were included in this analysis only if both α cells were able to be quantified at the timepoint following the birth of the second-born α cell.

(D) Example of a long birth-time interval. Quantitation of the nuclear Red:Green ratios over time for an individual with a long birth-time interval. The trajectory of the first-born α cell is indicated by a blue line and the second-born α cell by a red line; the birth-time interval in this case is 150 minutes (yellow double-arrowed line). The α cells are born with similar nuclear Red:Green ratios (solid blue and red stars), but by time the second-born α cell is born, the first-born α cell has a higher nuclear Red:Green ratio (blue outlined star), and the difference is sustained over time. The inset shows the α cells at the timepoint immediately following the birth of the second-born α cell. Scale bar is 4 μm.

(E) Examples of short birth-time intervals. Cells are represented as in D. The first- and second-born α cells have similar nuclear Red:Green ratios when they are born (solid stars). Left, the first-born α cell gains a LIN-12 advantage; right, the second-born α cell does (STAR Methods).

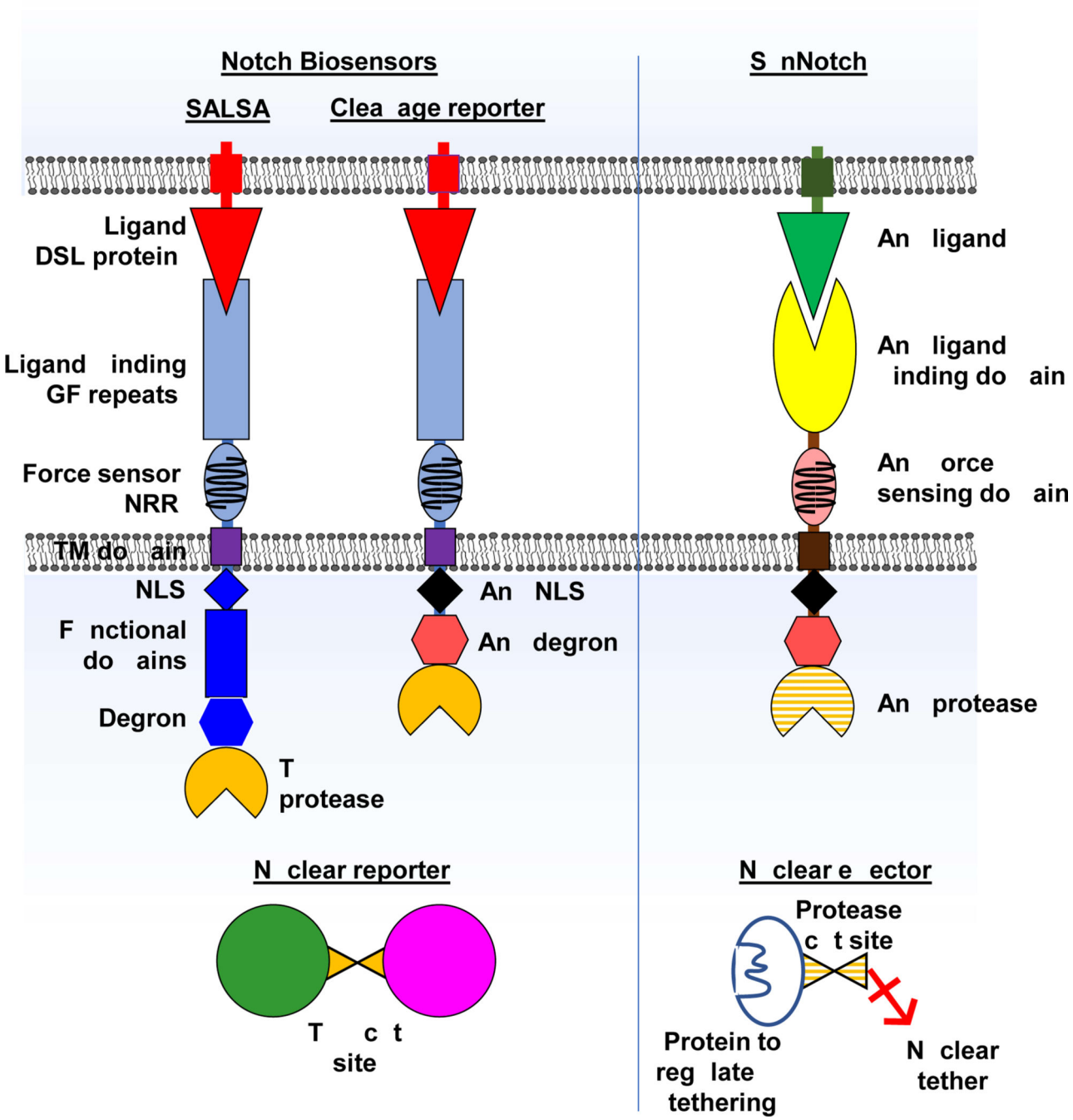

Figure 7. The modular design of the SALSA switch and reporter may be adapted for other potential applications.

Switch design: For this study, we used TEVp fused to the C-terminus of endogenous LIN-12/Notch, as our primary goal was to measure LIN-12 signaling activity during cell fate decisions. However, each component of the switch may be altered depending on the application, and any switch may be introduced as a transgene. For example, replacement of the ICD with an exogenous NLS, with or without an alternative degron, would remove native regulation of the active Notch intracellular domain for focusing on ligand, ADAM

protease, or Presenilin/γ-secretase activity. “SynNotch” proteins that have outputs other than transcriptional activation may be modeled on SALSA by using alternatives for any of the Notch domains, and TEVp or other protease moieties with an NLS, further tuned by presence or absence of a degron.

Reporter design: Modifications can change the purpose from reporting switch activity to regulating the activity of a nuclear-tethered protein. For example, tethering a cytosolic ubiquitin ligase or kinase using a histone or other nuclear anchor via the Tcut site would allow for conditional degradation or phosphorylation of specific cytosolic targets that is dependent upon switch activity, or tethering a pro-protein that is matured by cleavage at the protease cut site would allow for ligand-controlled regulation of its activity.

KEY RESOURCES TABLE

REAGENT or RESOURCE	SOURCE	IDENTIFIER
Chemicals, peptides, and recombinant proteins		
Tetramisole hydrochloride	Sigma Aldrich	T1512–2G
Ethyl 3-aminobenzoate methanesulfonate (tricaine)	Sigma Aldrich	E10521–10G
Experimental models: Organisms/strains		
C. elegans: N2: *C elegans*, Bristol Isolate	Caenorhabditis Genetics Center	RRID:WB-Strain: N2
C. elegans: GS8949: *hlh-2(ar623)[gfp::h2b] I*	Attner et al. (2019)	RRID:WB-Strain: GS8949
C. elegans: GS9215: *lin-12(ar640) III*	This paper	N/A
C. elegans: GS9324: *arTi351[lin-31p::gfp::tcut::mScarlet::h2b::unc-54 3'UTR] V:−12.74*	This paper	N/A
C. elegans: GS9338: *lin-12(ar640) III; arTi351 V*	This paper	N/A
C. elegans: GS9854: *hlh-2(ar614) I; lin-12(ar640) III; arTi351 V*	This paper	N/A
C. elegans: GS9339: *arTi356[lin-31p::gfp::tcut::mCherry::h2b::unc-54 3'UTR] I:−18.51; lin-12(ar640) III*	This paper	N/A
C. elegans: GS9452: *arTi356 I; arTi145[ckb-3p::mcherry::h2b] II; lin-12(ar640); sel-10(ar41) V; arTi22 [hlh-2prox::gfp] X*	This paper	N/A
C. elegans: GS9399: *arTi359[hlh-8p::gfp::tcut::mScarlet::h2b::unc-54 3'UTR] III:−0.45 lin-12(ar640) III*	This paper	N/A
C. elegans: GS9317: *arSi85[mex-5p::gfp::tcut::mCherry::h2b::tbb-2 3'UTR] I:−5.31*	This paper	N/A
C. elegans: GS9447: *arSi85 I; glp-1(ar648) III*	This paper	N/A
C. elegans: GS8795: *arTi237[ckb-3p::Cre(opti)::tbb-2 3'UTR] X:11.72*	Shaffer and Greenwald (2022)	N/A
C. elegans: GS9322: *arTi355 IV; arTi237 X*	This paper	N/A
C. elegans: GS9314: *lin-12(ar640) III; arTi355 IV; arTi237 X*	This paper	N/A
Software and algorithms		
ImageJ	Imagej.nih.gov	RRID:SCR_003070
MATLAB	Mathworks.com	RRID:SCR_001622
CellProfiler	CellProfiler.com	RRID:SCR_007358
Zen	Zeiss.com	RRID:SCR_013672
CellProfiler scripts used in this study, and Matlab script for nuclear tracking	Github.com/GreenwaldLab	de-la-Cova-2017
Matlab script for data extraction	Github.com/kluo91	Image-Quantification